Dystroglycan Maintains Inner Limiting Membrane Integrity to Coordinate Retinal Development

Reena Clements[1], Rolf Turk[3], Kevin P. Campbell[3], and Kevin M. Wright[1,2, #]

1) Neuroscience Graduate Program, 2) Vollum Institute, Oregon Health & Science University, Portland, OR 97239, USA, 3) Howard Hughes Medical Institute, Department of Molecular Physiology and Biophysics, Department of Neurology, Department of Internal Medicine, The University of Iowa Roy J. and Lucille A. Carver College of Medicine, Iowa City, IA USA.

#) Correspondence to Kevin M Wright (wrighke@ohsu.edu). Vollum Institute, 3181 SW Sam Jackson Park Rd L474 Portland, OR 97239. (503)-494-6955

Running Title:
Dystroglycan regulates retinal development

Abstract

Proper neural circuit formation requires the precise regulation of neuronal migration, axon guidance and dendritic arborization. Mutations affecting the function of the transmembrane glycoprotein dystroglycan cause a form of congenital muscular dystrophy that is frequently associated with neurodevelopmental abnormalities. Despite its importance in brain development, the precise role for dystroglycan in regulating retinal development remains poorly understood. Using a mouse model of dystroglycanopathy (*ISPD*^{L79*}) and conditional *dystroglycan* mutants, we show that dystroglycan is critical for the proper migration, axon guidance and dendritic stratification of neurons in the inner retina. Using genetic approaches, we show that dystroglycan functions in neuroepithelial cells as an extracellular scaffold to maintain the integrity of the retinal inner limiting membrane (ILM). Surprisingly, despite the profound disruptions in inner retinal circuit formation, spontaneous retinal activity is preserved. These results highlight the importance of dystroglycan in coordinating multiple aspects of retinal development.

Introduction

The precise lamination of neurons is a common organizing principle of the vertebrate nervous system and is critical for establishing proper connectivity. In many regions of the developing nervous system, newly generated neurons migrate in a basal direction away from apically located proliferative zones. In the developing retina, progenitor cells localized in the apical neuroepithelium undergo asymmetric cell divisions to produce a variety of retinal cell types in a sequential manner (Reese, 2011). Retinal ganglion cells (RGCs), the sole output cells of the retina, are generated first in early embryonic development, followed by horizontal cells and cones. Rods, amacrine cells, bipolar cells and Müller glia are the last to differentiate (Bassett and Wallace, 2012; Livesey and Cepko, 2001; Reese, 2011). In contrast to the developing cortex, birthdate order does not predict the laminar placement of neurons within the retina. Rather, the retina is organized in three major cellular layers: the apically located outer nuclear layer (ONL) comprised of rod and cone photoreceptors; the inner nuclear layer (INL) containing horizontal cells, bipolar cells and amacrine cells; and the basally located ganglion cell layer containing RGCs and displaced amacrine cells (Bassett and Wallace, 2012). Two synaptic lamina form postnatally in the retina: the outer plexiform layer (OPL), which contains synapses between photoreceptors, bipolar cells and horizontal cells; and the inner plexiform layer (IPL), which contains synapses between bipolar cells, amacrine cells and RGCs. The molecular cues that direct the stratification of neuronal subtypes and their processes in the retina remain poorly understood.

Unlike the cerebral cortex, where many neurons migrate along the radial glia scaffold, neuronal migration in the retina does not require contact between neurons and

neuroepithelial cells (Reese, 2011). RGCs, bipolar cells and photoreceptors migrate by nuclear translocation through a basally-directed process, while amacrine cells and horizontal cells migrate without obvious processes directed towards either the apical or basal surface of the retina. Basal process contact with the inner limiting membrane (ILM) is critical for the polarization and migration of RGCs (Randlett et al., 2011). RGC axons form in the optic fiber layer (OFL), along the laminin-enriched ILM, and direct their axon growth to the optic disc at the center of the retina (Bao, 2008). The ILM is made up of various extracellular matrix (ECM) proteins including laminins, Collagen IV, nidogens, perlecan, and agrin (Taylor et al., 2015; Varshney et al., 2015). Mutations in specific laminins (Lamα1, Lamβ2 and Lamγ3) or the laminin receptor β1-Integrin, disrupt formation of the ILM and organization of the ganglion cell layer (GCL) (Edwards et al., 2010; Gnanaguru et al., 2013; Pinzon-Duarte et al., 2010; Riccomagno et al., 2014). How laminins and other ECM proteins are initially organized in the ILM remains unclear.

In addition to β1-Integrin, the transmembrane glycoprotein dystroglycan functions as a receptor for laminins and other ECM proteins that contain Laminin G (LG) domains through its extracellular α-subunit. Dystroglycan also connects to the actin cytoskeleton through the intracellular domain of its transmembrane β-subunit, which is part of the dystrophin glycoprotein complex (Moore and Winder, 2010). The extensive glycosylation of dystroglycan's α-subunit is essential for its function, with the mature glycan chains binding to LG motifs present in a number of ECM proteins (Moore and Winder, 2012). Mutations in one of 17 genes encoding proteins required for the functional glycosylation of dystroglycan lead to a form of congenital muscular dystrophy termed dystroglycanopathy (Taniguchi-Ikeda et al., 2016). Patients with

dystroglycanopathy can present a wide range of symptoms, and the most severe forms, Muscle-Eye-Brain disease (MEB) and Walker Warburg Syndrome (WWS), are accompanied by significant neurological involvement (Godfrey et al., 2011). MEB and WWS are characterized by cortical malformation (type II lissencephaly), cerebellar abnormalities, and retinal dysplasias (Dobyns et al., 1989).

Cortical malformations in dystroglycanopathies have been well-studied, and reflect neuronal migration defects that arise from the critical role that dystroglycan plays in maintaining the architecture of the neuropithelial scaffold (Moore et al., 2002; Myshrall et al., 2012). In several mouse models of dystroglycanopathy, focal regions of retinal dysplasia have been observed, with ectopic cells protruding through the ILM (Chan et al., 2010; Lee et al., 2005; Satz et al., 2008; Takahashi et al., 2011; Takeda et al., 2003). However, several important questions regarding the role of dystroglycan in retinal development remain unaddressed. First, is dystroglycan required for the proper migration and lamination of specific subtypes of retinal neurons? Second, is dystroglycan required to maintain the ILM as a growth substrate for RGC axons as they exit the retina? Third, how does the loss of dystroglycan affect the postnatal dendritic stratification and mosaic spacing of retinal neurons? Finally, how do the retinal dysplasias present in models of dystroglycanopathy affect the function of the retina?

Here, using multiple genetic models, we identify a critical role for dystroglycan in multiple aspects of retinal development. We show that dystroglycan within the neuroepithelium is critical for maintaining the structural integrity of the ILM. We provide *in vivo* evidence that dystroglycan's maintenance of the ILM is required for proper neuronal migration, axon guidance and the postnatal formation of synaptic lamina

specifically within the inner retina. Surprisingly, spontaneous retinal activity appears unperturbed, despite the dramatic disruption in inner retinal development. Together, these results provide critical insight into how dystroglycan directs the proper functional assembly of retinal circuits.

Results

Dystroglycan is required for inner limiting membrane integrity and axon tract formation in the developing retina

Dystroglycan plays a critical role in the developing cortex, where it anchors radial neuroepithelial endfeet to the basement membrane along the pial surface. In the absence of functional dystroglycan, disruptions in the cortical basement membrane and detachment of neuroepithelial endfeet lead to profound neuronal migration phenotypes (Moore et al., 2002; Myshrall et al., 2012). In the adult retina, dystroglycan is present in blood vessels, in RGCs, at ribbon synapses in the OPL, and at the ILM, which serves as a basement membrane that separates the neural retina from the vitreous space (Montanaro et al., 1995; Omori et al., 2012). However, the role of dystroglycan in regulating neuronal migration, axon guidance or dendritic stratification of specific cell types during retinal development has not been examined in a comprehensive manner. To address this open question, we first examined the expression pattern of dystroglycan in the developing retina. Using immunohistochemistry, we observed dystroglycan expression along radial processes that span the width of the retina, and its selective enrichment at the ILM from embryonic ages (e13) through birth (P0) (Figure 1A). These processes are likely a combination of neuroepithelial cells and the basal process of migrating RGCs. Loss of staining in retinas from an epiblast-specific *dystroglycan*

conditional knockout (*DG$^{F/-}$; Sox2^{cre}*) confirmed the specificity of this expression pattern (Figure 1A).

The first step in the assembly of basement membranes is the recruitment of laminin polymers to the cell surface by sulfated glycolipids, followed by the stabilization of laminin polymers by transmembrane receptors (Yurchenco, 2011). To determine whether dystroglycan is required for the initial formation of the ILM during retinal development, we utilized two complementary genetic models. *ISPD$^{L79*/L79*}$* mutants, previously identified in a forward genetic screen, lack the mature glycan chains required for dystroglycan to bind ligands such as laminin and are a model for severe dystroglycanopathy (Wright et al., 2012). *DG$^{F/-}$; Sox2^{cre}* conditional mutants lack dystroglycan in all epiblast-derived tissues and were utilized to confirm that phenotypes observed in *ISPD$^{L79*/L79*}$* mice are dystroglycan dependent. The enrichment of laminin at the ILM appeared normal in early retinal development at e13 in both *ISPD$^{L79*/L79*}$* and *DG$^{F/-}$; Sox2^{cre}* mutants (Figure 1B-D), indicating that dystroglycan is not required for the initial formation of the ILM. However, at e16, we observed a profound loss of laminin staining and degeneration of the ILM across the entire surface of the retina in *ISPD$^{L79*/L79*}$* and *DG$^{F/-}$; Sox2^{cre}* mutants (Figure 1C-D, Supplemental Figure 1). The loss of ILM integrity in *ISPD$^{L79*/L79*}$* and *DG$^{F/-}$; Sox2^{cre}* mutants was accompanied by the inappropriate migration of retinal neurons, resulting in the formation of an ectopic layer of neurons protruding into the vitreous space.

Following the initial polymerization of laminin on cell surfaces, additional ECM proteins bind and crosslink the nascent basement membrane to increase its stability and complexity. Examination of *ISPD$^{L79*/L79*}$* mutant retinas at P0 revealed a loss of the

ECM proteins Collagen IV (red), and Perlecan (green), coinciding with the disruptions in Laminin (purple) (Figure 1E). These data suggest that while dystroglycan is not required for the initial formation of the ILM, it is essential for its maturation and maintenance. Furthermore, dystroglycan is critical for the ILM to function as a structural barrier to prevent the ectopic migration of neurons into the vitreous space.

The hyaloid vasculature in the embryonic retina normally regresses as the retinal vascular plexus emerges through the optic nerve head beginning around birth (Fruttiger, 2007). Previous studies have found that defects in ILM integrity disrupt retinal vasculature development (Edwards et al., 2010; Lee et al., 2005; Takahashi et al., 2011; Tao and Zhang, 2016). In agreement with these findings, we observe that at embryonic ages in *ISPD*$^{L79*/L79*}$ mutant retinas, the hyaloid vasculature becomes embedded within the ectopic retinal neuron layer (Supplemental Figure 2A), and fails to regress at P0 (Supplemental Figure 2B). In addition, the emergence of the retinal vasculature is stunted in *ISPD*$^{L79*/L79*}$ mutants (Supplemental Figure 2B). This is likely due to defects in the migration of astrocytes, which also emerge from the optic nerve head just prior to endothelial cells and require an intact ILM for their migration (Tao and Zhang, 2016).

We previously showed that the organization of the basement membrane by dystroglycan provides a permissive growth substrate for axons in the developing spinal cord (Wright et al., 2012). In addition, contact with laminin in the ILM stabilizes the leading process of newly generated RGCs to direct the formation of the nascent axon (Randlett et al., 2011). These axons remain in close proximity to the ILM as they extend centrally towards the optic nerve head, forming the OFL. Therefore, we examined whether the disruptions in the ILM affected the guidance of RGC axons in *ISPD*$^{L79*/L79*}$

and *DG$^{F/-}$; Sox2^{cre}* mutants. At e13, axons in both control and mutant retinas formed a dense and continuous network in the basal retina, directly abutting the ILM (Figure 2A). In contrast, at e16 (Figure 2B) and P0 (Figure 2C), RGC axons in *ISPD$^{L79*/L79*}$* and *DG$^{F/-}$; Sox2^{cre}* mutants were highly disorganized, exhibiting both defasciculation (asterisks) and hyperfasciculation (arrowheads).

To gain further insight into the specific defects that occur in RGC axons, we used a flat mount retina preparation. Regardless of their location in the retina, all RGCs orient and extend their axons towards the center of the retina, where they exit the retina through the optic nerve head (Bao, 2008). In control retinas at e16 (Figure 2D, left panel) and P0 (Figure 2E, left panel) axons traveled towards the optic nerve head in fasciculated, non-overlapping bundles. By e16 RGC axons in both *ISPD$^{L79*/L79*}$* and *DG$^{F/-}$; Sox2^{cre}* mutants were highly defasciculated and a large proportion frequently grew in random directions without respect to their orientation to the optic nerve head, resulting in their failure to exit the retina. However, it is important to note that some axons retained their appropriate centrally-orientated trajectory, which may be indicative of RGC axons that have already traversed the retina to the optic nerve head prior to the degeneration of the ILM (Figure 1) (Petros et al., 2008). Together, these data show that proper growth and guidance of RGC axons to the optic nerve head requires dystroglycan to maintain an intact ILM as a growth substrate.

Dystroglycan is required for axonal targeting, dendritic lamination, and cell spacing in the postnatal retina

Our results in *ISPD*$^{L79*/L79*}$ and *DG*$^{F/-}$*; Sox2*^{cre} mutants demonstrate that dystroglycan is required for ILM integrity and to prevent the ectopic migration of neurons into the vitreous (Figure 1), consistent with other models of dystroglycanopathy. However, the specific neuronal subtypes affected in models of dystroglycanopathy are unknown, and the role of dystroglycan in regulating postnatal aspects of retinal development has not been examined. The synaptic layers of the retina develop postnatally, with tripartite synapses between the photoreceptors, bipolar cells and horizontal cells forming in the OPL, and synapses between bipolar cells, amacrine cells and retinal ganglion cells forming in the IPL. The development of these synaptic layers requires the precise stratification of both axons and dendrites that occurs between P0 and P14. Since *ISPD*$^{L79*/L79*}$ and *DG*$^{F/-}$*; Sox2*^{cre} mutant mice exhibit perinatal lethality, we deleted *dystroglycan* selectively from the early neural retina and ventral forebrain using a *Six3*^{Cre} driver (Furuta et al., 2000) (Supplemental Figure 3).

We first confirmed that *DG*$^{F/-}$*; Six3*^{cre} mice recapitulated the retinal phenotypes identified in *ISPD*$^{L79*/L79*}$ and *DG*$^{F/-}$*; Sox2*^{cre} mice. We observed a degeneration of the ILM (laminin, purple) accompanied by ectopic migration of neurons into the vitreous, and abnormal fasciculation and guidance of RGC axons at P0 (Figure 3A-B). While fully penetrant, the ILM degeneration and neuronal migration defects in *DG*$^{F/-}$*; Six3*^{cre} mice were milder than in *DG*$^{F/-}$*; Sox2*^{cre} mice, exhibiting a patchiness that was distributed across the retina (Supplemental Figure 3C). The defects in *DG*$^{F/-}$*; Six3*^{cre} mice contrast the finding that conditional deletion of *dystroglycan* with *Nestin*^{cre} does not affect the overall structure of the retina (Satz et al., 2009). We find that this difference is likely due to the onset and pattern of *Cre* expression, as recombination of a *Cre*-

dependent reporter (*Rosa26-lox-stop-lox-TdTomato; Ai9*) occurred earlier and more broadly in *Six3*^{Cre} mice than in *Nestin*^{cre} mice (Supplemental Figure 3).

DG$^{F/-}$*; Six3*^{cre} mice are healthy and survive into adulthood, allowing us to examine the role of dystroglycan in postnatal retinal development. We analyzed *DG; Six3*^{cre} retinas at P14 when migration is complete and the laminar specificity of axons and dendrites has been established (Morgan and Wong, 1995). The overall architecture of the ONL appeared unaffected by the loss of dystroglycan in *DG*$^{F/-}$*; Six3*^{cre} mice, and cell body positioning of photoreceptors appeared similar to controls (Supplemental Figure 4). Within the INL, the laminar positioning of rod bipolar cell bodies (PKC, Figure 3C), cone bipolar cell bodies (SCGN, Figure 3D) and horizontal cells (arrows, Calbindin, Figure 3F) and the targeting of their dendrites to the OPL appeared normal in *DG*$^{F/-}$*; Six3*^{cre} mutants. However, bipolar cell axons that project towards the inner retina and are normally confined to the synaptic layers in the IPL extended aberrant projections into the ectopic clusters (Figure 3C).

In contrast, subsets of amacrine and ganglion cells labeled by ChAT (starburst amacrine cells, Figure 3E), calbindin (Figure 3F) calretinin (Figure 3G) that are normally confined to the INL and GCL were present in the ectopic clusters that protrude into the vitreous space. Glycinergic amacrine cells (GlyT1, Figure 3H), whose cell bodies are normally found in a single layer within the INL, were also present within ectopic clusters. Compared to the OPL, which appeared grossly normal, dendritic stratification within the IPL in *DG*$^{F/-}$*; Six3*^{cre} mutant retinas was highly disrupted. The normally tightly laminated dendritic strata appeared expanded (Figure 3E), fragmented (Figure 3E-G) and occasionally lacked an entire lamina (Figure 3F). These defects were restricted to

regions of the retina where ectopic neuronal clusters were present, whereas regions of the *DG$^{F/-}$; Six3^{cre}* mutant retina with normal cellular migration and lamination also had normal dendritic stratification (Supplemental Figure 3). These results demonstrate that the ectopic clusters consisted of multiple subtypes of amacrine cells and ganglion cells that normally reside in the INL and GCL, and that the disorganization of the dendritic strata are likely secondary to the cell migration defects.

Over the course of retinal development, multiple cell types, including horizontal cells and amacrine cells, develop mosaic spacing patterns that ensure cells maintain complete and non-random coverage over the surface of the retina (Wassle and Riemann, 1978). This final mosaic pattern is established by both the removal of excess cells through apoptosis and the lateral dispersion of “like-subtype” cells via homotypic avoidance mechanisms (Kay et al., 2012; Li et al., 2015). To determine whether the defects in establishing proper positioning of retinal subtypes in *DG$^{F/-}$; Six3^{cre}* mutants extends to mosaic spacing, we performed nearest neighbor analysis. For horizontal cells, which exhibit normal lamination in *DG$^{F/-}$; Six3^{cre}* mutant retinas, we observed a small, but significant reduction in cellular density (Figure 5F). Despite the reduction in the density of horizontal cells, nearest neighbor curves between controls and mutants are the same shape, indicating that horizontal cell mosaics are maintained in dystroglycan mutants (Figure 4A, B, Two-Way ANOVA, $p<0.01$).

ChAT positive starburst amacrine cells are present in two distinct lamina that form mosaic spacing patterns independent from one another. Consistent with this, ChAT labeled cells in the INL showed normal mosaic cell spacing (Figure 4C, top, Figure 4D, top, Two-Way ANOVA, $p>0.05$). In contrast, the GCL contained prominent ChAT

positive clusters that corresponded to the ectopic protrusions that extend into the vitreous, resulting in a decrease in cell spacing as determined by nearest neighbor analysis, (Figure 4C, bottom, Figure 4D, bottom, Two-Way ANOVA, $p<0.01$). These results demonstrate that laminar migration defects in *DG$^{F/-}$; Six3^{cre}* mutants degrade the mosaic spacing of cells in the GCL, and that contact with an intact ILM is likely required for the proper lateral dispersion of these cells.

Deletion of dystroglycan leads to a loss of photoreceptors, horizontal cells and ganglion cells

During development, normal physiological apoptotic cell death during the first two postnatal weeks plays an important role in retinal maturation (Young, 1984). This process is critical for establishing the proper numbers and spacing of some subtypes of cells across the mature retina, as well as removing cells that fail to connect to appropriate synaptic targets (Braunger et al., 2014). Degeneration of the ILM during development can lead to a reduction in the number of ganglion cells, and previous analysis of dystroglycanopathy mutants has noted thinning of the retina (Chan et al., 2010; Halfter et al., 2005; Lee et al., 2005; Satz et al., 2008; Takahashi et al., 2011). In agreement with these results, we observed that the retinas of *DG$^{F/-}$; Six3^{cre}* mutants are thinner (Figure 3, 5). However, the specific cell types affected by the loss of dystroglycan in the retina are unknown.

To investigate the mechanism by which loss of dystroglycan contributes to retinal thinning, we began by measuring the distance between the edges of the inner and outer retina in control and *DG$^{F/-}$; Six3^{cre}* mutants by DAPI staining and found that there was a

255 significant reduction in overall retinal thickness by approximately 20% in mutants
256 (Figure 5A, blue, Figure 5B, t test, $p<0.01$). We next investigated which specific cell
257 types contribute to retinal thinning. In the outer retina, the thickness of the photoreceptor
258 layer (recoverin, Figure 5A, green, Figure 5C, t-test, $p<0.05$) was reduced by
259 approximately 20% and the density of horizontal cells had a small, yet significant
260 reduction in *DG$^{F/-}$; Six3^{cre}* mutants (calbindin, Figure 5F, t-test, $p<0.05$). In contrast, the
261 thickness of the bipolar cell layer (Chx10, Figure 5A, purple, Figure 5D, t-test, $p<0.05$)
262 was normal. In the inner retina, there was a 50% reduction in the density of ganglion
263 cells (Figure 5G, H, t-test, $p<0.0001$), while the density of ChAT+ starburst amacrine
264 cells in both the GCL and INL was normal in *DG$^{F/-}$; Six3^{cre}* mutants (Figure 5E, t-test,
265 $p<0.05$). Thus, the loss of photoreceptors, horizontal cells and RGCs contribute to the
266 overall thinning of the retina.

267 To determine whether the reduction in photoreceptors, horizontal cells and RGCs in
268 the absence of dystroglycan was the result of increased cell death, we examined early
269 postnatal ages when normal physiological apoptosis occurs in the retina. In *DG$^{F/-}$;*
270 *Six3^{cre}* mutants at P0, we observed an increased number of cleaved caspase-3 positive
271 cells that was restricted to the ganglion cell layer (Figure 5I, J, t-test, $p<0.05$) and was
272 not observed in other layers of the retina (data not shown). We also examined
273 *ISPD$^{L79*/L79*}$* mutants to assess GCL apoptosis in a dystroglycanopathy model. Prior to
274 the normal period of physiological apoptosis in the retina we observed a massive
275 increase in caspase-3 positive cells at e16 in mutants (Figure 5J t-test, $p<0.0001$) that
276 continued through P0 (Figure 5I, J, t-test, $p<0.0001$). These results led us to conclude

that the dramatic loss of RGCs in *DG$^{F/-}$; Six3^{cre}* mutants is due to increased apoptotic cell death.

Dystroglycan functions non-cell autonomously as a scaffold in the developing retina

We next sought to provide mechanistic insight into how dystroglycan regulates retinal development *in vivo*. In the cerebral cortex, the loss of dystroglycan results in breaches of the pial basement membrane and detachment of neuroepithelial endfeet from the pial surface, depriving neurons of a migratory scaffold. In addition, the cortical basement membrane defects cause the mis-positioning of Cajal-Retzius cells, which are the source of Reelin that regulates somal translocation of neurons as they detach from the neuroepithelial scaffold (Nakagawa et al., 2015). Deletion of *dystroglycan* specifically from postmitotic neurons does not result in a migration phenotype (Satz et al., 2010), supporting a model in which the cortical migration phenotypes arise due to disrupted interactions between the basement membrane and neuroepithelial scaffold. In contrast to the cerebral cortex, the basal migration of RGCs does not involve contact with the neuroepithelial scaffold. Instead, newly born RGCs migrate via somal translocation using an ILM-attached basal process that eventually becomes the nascent axon (Icha et al., 2016; Randlett et al., 2011). Dystroglycan's expression in RGCs (Montanaro et al., 1995), and the restriction of neuronal migration and axon guidance defects to the GCL raise the possibility that dystroglycan could be functioning cell-autonomously in the basal processes of newly born RGCs. To test this possibility, we generated *DG$^{F/-}$; Isl1^{cre}* conditional knockouts. *Islet1* is expressed in the majority of

ganglion cells as they differentiate from the retinal progenitor pool (Pan et al., 2008). Analysis of *Isl1^{cre}* mice at e13 confirmed recombination occurs in the majority of newly born ganglion cells, but not in neuroepithelial progenitors (Supplemental Figure 5). Examination of *DG$^{F/-}$; Isl1^{cre}* mutants indicated that deletion of *dystroglycan* selectively from RGCs did not affect ILM integrity (Figure 6A, middle panel). Neuronal migration (Figure 6A, C and D, middle panels), axon guidance (Figure 6A and B, middle panels) and the stratification of dendrites in the IPL (Figures 6 C-D, middle panels) all appeared normal in *DG$^{F/-}$; Isl1^{cre}* mutants. These results demonstrate that dystroglycan is not required within RGCs themselves during retinal development.

Dystroglycan consists of two subunits that play distinct roles in the overall function of the protein. The extracellular α-subunit is heavily glycosylated and functions as an extracellular scaffold by binding to extracellular matrix components such as laminin. The β-subunit contains a transmembrane and intracellular domain, and can bind directly to dystrophin and other modifiers of the actin cytoskeleton as well as initiate intracellular signaling cascades (Moore and Winder, 2010). The intracellular domain of dystroglycan is required for the localization of dystrophin to the ILM, and mice lacking the intracellular domain of dystroglycan (*DG$^{-/\beta cyt}$*) (Satz et al., 2009) or the predominant retinal isoform of dystrophin (*Mdx^{3Cv}*) (Blank et al., 1999) have abnormal scotopic electroretinograms, suggesting a defect in retinal function. While these mice do not have any disruptions in the ILM or gross malformations in the retina, whether dystroglycan signaling through dystrophin is required for neuronal migration, axon guidance or dendritic stratification has not been examined. Consistent with the original report, examination of the ILM and overall architecture of the retina is normal in *DG$^{-/\beta cyt}$* mice. In addition, we find that

neuronal migration, axon guidance and stratification of dendritic lamina are unaffected in *DG*$^{-/\beta cyt}$ mice (Figure 6A-D, right panel). Therefore, intracellular signaling, including through dystrophin, is not required for these aspects of retinal development. Taken together with our results in *DG*$^{F/-}$*; Isl1*^{cre} mutants, these findings indicate that dystroglycan primarily functions in neuroepithelial cells as an extracellular scaffold to regulate the structural integrity of the ILM. The progressive degeneration of the ILM then leads to secondary defects including aberrant migration, axon guidance and dendritic stratification that primarily affect the inner retina.

Dystroglycan is dispensable for the generation of spontaneous retinal waves

One of the critical functions for laminar targeting in neural circuit development is to ensure that the axons and dendrites of appropriate cell types are in physical proximity to one another during synaptogenesis. In addition to regulating the laminar positioning of neurons in the cortex and retina, dystroglycan is required for the development of a subset of inhibitory synapses in the brain (Fruh et al., 2016). Therefore, we investigated the possibility that the loss of dystroglycan disrupts synapse formation in the retina. Previous studies have shown that ribbon synapses in the OPL are dysfunctional in the absence of dystroglycan or its ligand pikachurin (Sato et al., 2008). These synapses are normal at the resolution of light microscopy, but electron microscopy reveals that dystroglycan and pikachurin are required for the insertion of bipolar cell dendrite tips into ribbon synapse invaginations (Omori et al., 2012). Consistent with these results, we found that pre- and post-synaptic markers for ribbon synapses appear normal at the resolution of light microscopy (Figure 7A). In the inner retina, markers for excitatory

346 synapses (VGLUT1, Figure 7B) and inhibitory synapses (VGAT, Figure 7C) were
347 present in the IPL, but were also present in the mis-localized ectopic cell clusters that
348 protrude into the vitreous (asterisks). This finding is similar to a recent study in which
349 mice lacking the Cas family of intracellular adaptor proteins express synaptic markers
350 localized to aberrant neuronal ectopia that protrude into the vitreous (Riccomagno et al.,
351 2014). Therefore, these results suggest that mis-laminated neurons in the retina are
352 still able to recruit synaptic partners, despite their abnormal location.

353 The presence of synaptic markers in ectopic neuronal clusters in the inner retina
354 does not guarantee normal function of these neurons. Recording synaptic activity in
355 RGCs in response to light stimuli in *DG$^{F/-}$; Six3^{cre}* mutants is not feasible due the
356 requirement for dystroglycan at photoreceptor ribbon synapses. We instead analyzed
357 retinal waves, which are spontaneous bursts of activity that propagate across the retina
358 prior to eye opening and are independent of light stimulation. During early postnatal
359 development, these waves are initiated by acetylcholine (ACh) release from starburst
360 amacrine cells and propagate along the starburst amacrine cell network prior to
361 transmission to RGCs (Xu et al., 2016). In *DG$^{F/-}$; Six3^{cre}* mutants, ChAT positive
362 starburst amacrine cells are present in normal numbers, and while they are normally
363 localized and mosaically spaced in the INL, they are profoundly disorganized in the
364 GCL. Therefore, we expected that these defects might affect the propagation of retinal
365 waves through the starburst amacrine cell and RGC network. As disruptions in the ILM
366 in *DG$^{F/-}$; Six3^{cre}* mutants would lead to unequal loading of cell permeable calcium
367 indicators, we utilized the genetically-encoded calcium indicator GCaMP6f crossed onto
368 the *DG; Six3^{cre}* line to visualize retinal waves.

Retinal waves in control *DG$^{F/+}$; Six3^{cre}; R26-LSL-GCaMP6f* retinas at P1-P2 were robust and had similar spatiotemporal features (size, rate of propagation, refractory period) to waves measured using cell-permeable calcium indicators (Arroyo and Feller, 2016). Consistent with previous reports, there is a broad distribution of wave size in control retinas (Figures 8A, 8C). Neighboring waves do not overlap with one another, but rather tile the retinal surface during the two-minute imaging period. To our surprise, retinal waves were present and appeared grossly normal in *DG$^{F/-}$; Six3^{cre}; R26-LSL-GCaMP6f* mutants (Figure 8B, D). Waves in control and mutant retinas exhibited a similar distribution in wave size (Figure 8 E, F), and the average wave size showed no statistical difference. The rate of wave propagation showed a similar distribution between controls and mutants. The average rate of wave propagation showed a small, but statistically significant, decrease (Wilcoxon Rank Sum test, $p<0.05$). Thus, despite the dramatic disorganization of ChAT positive starburst amacrine cells in the GCL of *DG$^{F/-}$; Six3^{cre}* mutants, the generation and propagation of retinal waves persisted.

Discussion

Defects in retinal structure and function are commonly observed in human patients with dystroglycanopathy, and are recapitulated in mouse models of dystroglycanopathy (Chan et al., 2010; Lee et al., 2005; Satz et al., 2008; Satz et al., 2009; Takahashi et al., 2011; Takeda et al., 2003). However, the mechanism of dystroglycan function in the retina and the consequence of its loss on specific cell types are poorly understood. Our study establishes a critical role for dystroglycan in regulating neuronal migration in order to establish laminar architecture and mosaic spacing in the inner retina. In the absence

of functional dystroglycan, the retinal ILM undergoes rapid and progressive degeneration, leading to the formation of cellular ectopias in the vitreous space and defects in intraretinal axon guidance. In the postnatal retina, these migration defects result in the mis-localization of multiple subtypes of GCL and INL cells into cellular ectopias and disrupt the mosaic spacing of cells in the GCL. Mechanistically, we show that these defects are exclusively due to dystroglycan's function as an extracellular scaffold, as mice lacking the intracellular domain of dystroglycan (*DG*$^{-/\beta cyt}$) appear phenotypically normal. Furthermore, dystroglycan functions non-cell autonomously, as selective deletion of *dystroglycan* from postmitotic RGCs (*DG; Isl1*^{cre}) did not affect ILM integrity, neuronal migration or axon guidance. Despite the dramatic disruptions in cellular lamination in the GCL and dendritic stratification in the IPL in *DG; Six3*^{cre} mutants, dystroglycan appears dispensable for the formation of synapses and the generation of spontaneous, light-independent activity in the retina.

Temporal requirement for dystroglycan during retinal development.

Using two genetic models for the complete loss of functional dystroglycan (*ISPD*^{L79*} and *DG; Sox2*^{Cre}), we demonstrated that after the ILM forms, it rapidly degenerates in the absence of dystroglycan. In *DG; Six3*^{cre} mutants, in which broad recombination occurs throughout the retina by e13, a milder degeneration of the ILM occurs. In contrast, the ILM appears grossly normal in *DG; Nestin*^{cre} mutants in which broad recombination does not occur until later stages (Satz et al., 2009) (Supplemental Figure 3). These results suggest that dystroglycan is not required for the formation of the

nascent ILM, but rather plays a critical, yet transient, role in maintaining ILM structure as it expands to accommodate the growing retina.

Recruitment of laminin is a critical early step in the assembly of the ILM, and several laminin mutants have disruptions in ILM integrity (Edwards et al., 2010; Gnanaguru et al., 2013; Pinzon-Duarte et al., 2010). The localization of laminin to the early ILM even in the complete absence of dystroglycan raises the possibility that other laminin receptors, such as β-1 Integrin, may compensate for the loss of dystroglycan. Mice lacking β-1 Integrin in the retina exhibit a similar defect to *dystroglycan* mutants, with normal ILM formation followed by rapid degeneration, supporting the possibility of redundancy between dystroglycan and β-1 Integrin (Riccomagno et al., 2014). Surprisingly however, mice in which both dystroglycan and β-1 Integrin are deleted from the retina (*DG*; *ItgB1*; *Six3*^{Cre}) still formed an ILM, and exhibited similar phenotypic severity to *DG*; *Six3*^{Cre} mutant retinas (unpublished observations). These results demonstrate that both dystroglycan and β-1 Integrin are dispensable, and sulfated glycolipids alone are likely sufficient for the recruitment of laminin during the initial formation of the ILM.

The ILM is required for neuronal migration in the retina

The role of dystroglycan has been extensively studied in the developing cortex, where it regulates the attachment of the radial glial endfeet to the pial basement membrane (Myshrall et al., 2012). The degeneration of the radial glia processes and the ectopic clustering of Cajal-Retzius neurons, the primary source of reelin in the developing cortex, are the earliest observable pathological features in models of

438 dystroglycanopathy (Booler et al., 2016; Nakagawa et al., 2015). The loss of a radial
439 migration scaffold and the abnormal distribution of reelin are thought to be the principal
440 drivers of structural brain defects in dystroglycanopathy. In contrast to the cortex, birth
441 order does not predict the laminar positioning of retinal neurons, retinal neuron
442 migration does not involve contact with the neuroepithelial scaffold, and there is no cue
443 analogous to reelin to signal the termination retinal neuron migration. Therefore, while
444 our results demonstrate that dystroglycan functions primarily in neuroepithelial cells in
445 the retina, the functional implications are distinct from its role in cortical neuroepithelial
446 cells.

447 We find that while dystroglycan is required to establish the proper architecture of the
448 retina, it appears that only amacrine cells and RGCs are affected. What is the driving
449 force behind the selective localization of amacrine cells and RGCs to the ectopic
450 clusters that protrude into the vitreous? Previous work has shown that elimination of
451 RGCs does not dramatically affect the lamination of other retinal neurons or the overall
452 architecture of the retina (Kay et al., 2004; Wang et al., 2001). However, if RGCs are
453 selectively mis-localized, other retinal neurons will organize themselves around the
454 displaced RGCs, resulting in an overall disorganization of retinal lamination (Icha et al.,
455 2016). In *dystroglycan* mutants, RGCs are the first neurons to encounter the
456 degenerating ILM and inappropriately migrate into the vitreous. Mis-localized RGCs
457 may then act actively recruit later born neurons such as amacrine cells to inappropriate
458 locations. Consistent with previous results observed in β-1 Integrin mutants, synaptic
459 markers were present in ectopic clusters, suggesting that neurons retain the ability to
460 recruit synaptic partners despite their inappropriate location (Riccomagno et al., 2014).

Many neurons migrate radially to their appropriate lamina, then undergo tangential migration to establish non-random mosaic patterns (Galli-Resta et al., 1997; Reese et al., 1999). This tangential migration involves interactions between immature neurites of neighboring cells (Galli-Resta et al., 2002; Huckfeldt et al., 2009) and short-range interactions mediated by DSCAM and MEGF10/11 (Fuerst et al., 2008; Kay et al., 2012). A key feature of this process is that it occurs between homotypic cells within the same lamina, and cells in which mosaic spacing is disrupted are no longer restricted to a two-dimensional plane. In *dystroglycan* mutants, the mosaic spacing of horizontal cells and INL starburst amacrine cells is normal, but is dramatically disrupted in starburst amacrine cells in the GCL. This defect is not due to dystroglycan functioning within starburst amacrine cells, as mosaic spacing was normal in *DG*; *Isl1*^{Cre} mutant retinas (data not shown). Rather, the selective defects in mosaic spacing of GCL starburst amacrine cells suggests that this may be a consequence of disrupting the two-dimensional organization of the GCL. Alternatively, mosaic spacing of cells within the GCL may require cues present in the ILM to guide tangential dispersion.

Intraretinal axon growth and guidance requires an intact ILM

Previous work has shown that the ILM and other basement membranes function as excellent growth substrates for extending axons (Halfter et al., 1987; Wright et al., 2012). Basement membranes are highly dynamic structures that not only contain pro-growth ECM molecules such as laminins and collagens, but also regulate the distribution of secreted axon guidance cues in the extracellular environment (Chai and Morris, 1999; Wright et al., 2012; Xiao et al., 2011). A number of secreted cues direct

intraretinal axon guidance of RGCs. Deletion of Netrin (Deiner et al., 1997) specifically affects exit of RGC axons through the optic nerve head, and deletion of Slits (Thompson et al., 2006) or Sfrps (Nieto-lopez et al., 2015) leads to the invasion of RGC axons into the outer retina. These specific phenotypes are distinct from those we observed in the absence of dystroglycan. The randomized growth and defasciculation of axons we observed in *ISPD*^{L79*} and *DG*; *Six3*^{Cre} mutant retinas is more consistent with defects observed upon deletion of adhesion receptors such as L1 (Bastmeyer et al., 1995), NCAM (Brittis et al., 1995) or DM-GRASP (Ott et al., 1998). These results suggest that the role of dystroglycan in guiding axons along the ILM is primarily to regulate axonal adhesion. While there are extensive intraretinal axon guidance defects in the absence of dystroglycan, some axons still appear normally oriented and fasciculated, exit the optic nerve head and project to the optic chiasm (Figure 2, unpublished results). We hypothesize that these normally oriented axons emanate from early born RGCs that begin to extend their axons as early as e13, prior the degeneration of the ILM. In contrast, later born RGCs that initiate axon growth after ILM degeneration lack an appropriate growth substrate and fail to orient their axons to the optic nerve head.

Loss of RGCs, photoreceptors and horizontal cells in the absence of dystroglycan

Previous studies of mouse models of dystroglycanopathy have consistently noted retinal thinning. However, based on these studies, it was unclear which retinal cell types were affected. Our comprehensive analysis of P14 *DG; Six3*^{cre} mutant retinas found that bipolar layer thickness was normal and INL and GCL starburst amacrine cells were

present at normal numbers. In contrast, photoreceptor layer thickness was reduced by approximately 20%, horizontal cell number in the INL was reduced by 16%, and RGC number exhibited a dramatic 50% reduction (Figure 5).

Analysis of e16 and P0 retinas from *ISPD*^{L79*} and *DG; Six3*^{cre} mutants indicated that the loss of RGCs was due to increased apoptosis of cells in the GCL that preceded and extended into the normal window of developmental apoptotic cell death. This increase in apoptotic cell death did not persist in adult (P56) *DG; Six3*^{cre} mutants (data not shown), suggesting it was likely restricted to the developing retina. Why are RGCs selectively lost at such a high rate in *DG; Six3*^{cre} mutants? One possibility is that the degeneration of the ILM selectively affects cells in the ganglion cell layer (ganglion cells and displaced amacrine cells). However, amacrine cell number remained unchanged in the GCL. Another possibility is that RGCs are selectively affected since they are the only cell type to project out of the retina. Indeed, we observed profound defects in the ability of RGC axons to navigate the optic chiasm in *ISPD*^{L79*} and *DG; Six3*^{cre} mutants (unpublished observations). These results suggest that the failure to reach retinorecipient regions of the brain resulted in the death of RGCs. It was originally postulated that BDNF from retinorecipient regions of the brain signaling through the TrkB receptor on RGCs regulates the survival of RGCs during development. However, RGC survival is unaffected in TrkB and BDNF knockouts (Cellerino et al., 1997; Rohrer et al., 2001). Therefore, while our data is consistent with the need for target-derived factors to support the survival of RGCs during development, the identity of these molecules remains elusive.

We also observed a reduction in thickness of the photoreceptor layer and in the number of horizontal cells in *DG; Six3^{cre}* mutants. While we did not observe increased caspase-3 reactivity in these cells at P0, it is possible that the loss of cells occurred gradually during the first two postnatal weeks. Dystroglycan is required for the proper formation of ribbon synapses between photoreceptors, horizontal cells and bipolar cells in the OPL (Omori et al., 2012; Sato et al., 2008). Therefore, the loss of appropriate synaptic contact in the absence of dystroglycan may lead to the elimination of a proportion of photoreceptors and horizontal cells.

Persistence of retinal waves in the absence of dystroglycan

The profound defects in lamination and dendritic stratification of ChAT positive starburst amacrine cells in *DG; Six3^{cre}* mutants led us to hypothesize that this would affect their ability to generate retinal waves. These waves are initiated by the spontaneous activity of starburst amacrine cells, independent of light stimuli, allowing us to circumvent the requirement for dystroglycan in proper transmission at ribbon synapses. Contrary to our expectations, retinal waves were present and propagated normally in *DG; Six3^{cre}* mutants (Figure 8). The persistence of retinal waves even in the context of disrupted starburst amacrine cell organization supports the model that these waves are the product of volume release of ACh from starburst amacrine cells that can trigger extra-synaptic responses (Ford et al., 2012). Using a cell-based sensor, Ford and colleagues detected ACh release several micrometers above the surface of the retina, suggesting that Ach diffusion is sufficient to trigger a response in cells that are not physically connected. Therefore, the relatively normal organization of INL starburst

552 amacrine cells may be sufficient to overcome the disorganization of GCL starburst
553 amacrine cells. We did observe a slight reduction in the rate of wave propagation, which
554 may be due to the reduced density of cells with calcium transients within a retinal wave
555 that were observed in *DG; Six3^{cre}* mutants. This reduced density likely reflects the
556 nearly 50% reduction in ganglion cell number, and suggests that while a full
557 complement of RGCs is not required for the propagation of retina waves, it may affect
558 their rate of propagation. While our results demonstrate that synaptic markers are
559 present in the inner retina and spontaneous retinal activity persists in *DG; Six3^{cre}*
560 mutants, it remains unknown whether synaptic transmission between specific cell types
561 within the inner retina is affected by the absence of dystroglycan.

562 Taken together, our data demonstrate that dystroglycan is required for multiple
563 aspects of retinal development. Similar to its role in the cortex, dystroglycan in the
564 retina functions within neuroepithelial cells to regulate the structural integrity of a
565 basement membrane (the ILM), which is required for the coordination of neuronal
566 migration, axon guidance and dendritic stratification in the inner retina. Overall, our data
567 suggest that the disorganization of the inner retina and the loss of photoreceptors,
568 horizontal cells and RGCs are key contributors to visual impairment in
569 dystroglycanopathy.

570

571 **Experimental Procedures**

572

573 **Animals**

574 Animal procedures were approved by OHSU Institutional Animal Care and Use
575 Committee and conformed to the National Institutes of Health *Guide for the care and*

use of laboratory animals. Animals were euthanized by administration of CO_2. The day of vaginal plug observation was designated as embryonic day 0 (e0) and the day of birth in this study was designated as postnatal day 0 (P0). The generation and genotyping protocols for *ISPD*$^{L79*/L79*}$ (Wright et al., 2012), *DG*$^{F/F}$ (Moore et al., 2002) and *DG*$^{\beta cyt}$ (Satz et al., 2009) mice have been described previously. The presence of the cre allele in *Six3*^{Cre} (Furuta et al., 2000), *Isl1*^{Cre} (Yang et al., 2006) and *Nestin*^{Cre} mice (Tronche et al., 1999) was detected by generic cre primers. *ISPD*$^{+/L79*}$, *DG*$^{\square\beta/+}$, and *DG*$^{F/+}$*; Six3*^{Cre} or *DG*$^{F/+}$ age matched littermates were used as controls.

Tissue Preparation and Immunohistochemistry

Embryonic retinas were left in the head and fixed overnight at 4°C in 4% PFA and washed in PBS for 30 minutes. Heads were equilibrated in 15% sucrose overnight and flash frozen in OCT medium. Postnatal retinas were dissected out of the animal and the lens was removed from the eyecup. Intact retinas were fixed at room temperature for 30 minutes in 4% PFA. Retinas were washed in PBS for 30 minutes and equilibrated in a sequential gradient of 10%, sucrose, 20% sucrose and 30% sucrose overnight. Tissue was sectioned on a cryostat at 16-25um. Tissue sections were blocked in a PBS solution containing 2% Normal Donkey Serum and 0.2% Triton for 30 minutes, and incubated in primary antibody overnight at 4°C. Sections were washed for 30 minutes and incubated in secondary antibody in a PBS solution containing 2% Normal Donkey Serum for 2-4 hours. Sections were incubated in DAPI to stain nuclei for 10 minutes, washed for 30 minutes, and mounted using Fluoromount medium. All immunohistochemistry images have $n \geq 3$ from at least two different litters of mice. The

source and concentration of all antibodies utilized in this study are listed in Supplemental Table 1.

Wholemount retinal staining

Postnatal retinas were dissected out of the animal and the lens was removed from the eyecup. Intact retinas were fixed at room temperature for 30 minutes in 4% PFA. Retinas were incubated in primary antibody diluted in PBS solution containing 2% Normal Donkey Serum and 0.2% Triton for two days at 4°C. Retinas were washed in PBS for one day and incubated in secondary antibody diluted in PBS solution containing 2% Normal Donkey Serum for two days at 4°C, washed for one day in PBS and mounted using Fluoromount medium.

Microscopy

Imaging was performed on a Zeiss Axio Imager M2 upright microscope equipped with an ApoTome.2. Imaging of synapses was performed on a Zeiss Elyra PS.1 with LSM 710 laser-scanning confocal Super-Resolution Microscope with AiryScan. Imaging of retinal waves was performed on a Nikon TiE inverted microscope with full environmental chamber equipped with a Yokogawa CSU-W1 spinning disk confocal unit.

Quantification of cell number and mosaic spacing

For each experiment, 3-4 locations per retina at the midpoint of each lobe were sampled. Cell counts of horizontal cells (Calbindin), apoptotic cells (Cleaved Caspase-3, P0), and starburst amacrine cells (ChAT) were obtained from 500 x 500 μm images and quantified in FIJI. Cell counts of apoptotic cells (Cleaved Caspase-3, e16) and ganglion cells (RPBMS) were obtained from 250 x 250 μm images and quantified in FIJI. Analysis of retinal mosaics (Calbindin, ChAT) were conducted on 500 x 500 μm images

by measuring the X-Y coordinates for each cell and Veronoi domains were calculated in Fiji and nearest neighbor measurements calculated with WinDRP.

Live cell imaging and analysis

Retinas from P1 *$DG^{F/+}$; $Six3^{cre}$; R26-LSL-GCaMP6f* and *$DG^{F/-}$; $Six3^{cre}$; R26-LSL-GCaMP6f* were dissected into chilled Ames' Medium (Sigma) buffered with sodium bicarbonate and bubbled with carbogen gas (95% O_2, 5% CO_2). The retinas were dissected out of the eyecup, mounted RGC side up on cellulose membrane filters (Millipore) and placed in a glass-bottom petri dish containing Ames' Medium. A platinum harp was used to stabilize the filter paper during imaging. Imaging was performed at 30°C using a 10x0.45 Plan Apo Air objective with a field of 1664 by 1404 μm with a 3Hz imaging timeframe. The field was illuminated with a 488 nm laser. 3-4 retinal fields were imaged per retina, and each field of retina was imaged for a two-minute time series using a 300ms exposure and each field was sampled 3-5 times per imaging session.

Thirty representative control and thirty representative mutant time series were randomly selected for analysis. Only waves that initiated and terminated within the imaging field were used for analysis. To measure wave area, movies were manually viewed using FIJI frame by frame to determine the start and end frame of a wave. A Z-Projection for maximum intensity was used to create an image with the entire wave, and the boundary of the wave was manually traced to determine the area. Wave area per time was calculated by dividing the area of the wave by the duration in seconds of the wave. Any wave lasting less than 2 seconds was not used in analysis, consistent with previous studies (Blankenship et al., 2009).

Statistics

644 Statistical analysis was performed using JMP Pro 13.0 software (SAS Institute).
645 Comparison between two groups was analyzed using a Student's t-test. Comparison
646 between two or more groups was analyzed using a Two-Way ANOVA and Tukey post-
647 hoc test. Comparison of retinal wave parameters was analyzed using a Wilcoxon Rank
648 Sums test. The significance threshold was set at 0.05 for all statistical tests. * indicates
649 $p<0.05$; ** indicates $p<0.01$; *** indicates $p<0.001$.
650

651 **Acknowledgements**

652 We thank Patrick Kerstein and Kylee Rosette for their technical assistance; Marla Feller
653 and Franklin Caval-Holme for advice on visualizing and analyzing retinal waves; W.
654 Rowland Taylor and Teresa Puthussery and members of their labs for antibodies and
655 technical advice; David Pow for the GlyT1 antibody; Catherine Morgans for the mGluR6
656 antibody, Stefanie Kaech Petrie and the OHSU Advanced Light Microscopy Core (ALM)
657 for assistance with confocal imaging; Alex Kolodkin, Martin Riccomagno, Randall Hand
658 and members of the Campbell and Wright laboratories for discussion throughout the
659 course of this study and comments on the manuscript. This work was supported by NIH
660 Grants R01-NS091027 (K.M.W.), The Medical Research Foundation of Oregon
661 (K.M.W.), NSF GRFP (R.C.), LaCroute Neurobiology of Disease Fellowship (R.C.),
662 Tartar Trust Fellowship (R.C.), NINDS P30–NS061800 (OHSU ALM), and a Paul D.
663 Wellstone Muscular Dystrophy Cooperative Research Center grant to K.P.C.
664 (1U54NS053672). K.P.C. is an investigator of the Howard Hughes Medical Institute

References

Arroyo, D.A., and Feller, M.B. (2016). Spatiotemporal Features of Retinal Waves Instruct the Wiring of the Visual Circuitry. Front Neural Circuits *10*, 54. PMC4960261. 10.3389/fncir.2016.00054

Bao, Z.Z. (2008). Intraretinal projection of retinal ganglion cell axons as a model system for studying axon navigation. Brain Research *1192*, 165-177. 10.1016/j.brainres.2007.01.116

Bassett, E.A., and Wallace, V.A. (2012). Cell fate determination in the vertebrate retina. Trends in neurosciences *35*, 565-573. 10.1016/j.tins.2012.05.004

Bastmeyer, M., Ott, H., Leppert, C.A., and Stuermer, C.A. (1995). Fish E587 glycoprotein, a member of the L1 family of cell adhesion molecules, participates in axonal fasciculation and the age-related order of ganglion cell axons in the goldfish retina. J Cell Biol *130*, 969-976. PMC2199948

Blank, M., Koulen, P., Blake, D.J., and Kroger, S. (1999). Dystrophin and beta-dystroglycan in photoreceptor terminals from normal and mdx3Cv mouse retinae. Eur J Neurosci *11*, 2121-2133

Blankenship, A.G., Ford, K.J., Johnson, J., Seal, R.P., Edwards, R.H., Copenhagen, D.R., and Feller, M.B. (2009). Synaptic and extrasynaptic factors governing glutamatergic retinal waves. Neuron *62*, 230-241. PMC2807181. 10.1016/j.neuron.2009.03.015

Booler, H.S., Williams, J.L., Hopkinson, M., and Brown, S.C. (2016). Degree of Cajal-Retzius Cell Mislocalization Correlates with the Severity of Structural Brain Defects in Mouse Models of Dystroglycanopathy. Brain Pathology *26*, 465-478. 10.1111/bpa.12306

Braunger, B.M., Demmer, C., and Tamm, E.R. (2014). Programmed cell death during retinal development of the mouse eye. Adv Exp Med Biol *801*, 9-13. 10.1007/978-1-4614-3209-8_2

Brittis, P.A., Lemmon, V., Rutishauser, U., and Silver, J. (1995). Unique changes of ganglion cell growth cone behavior following cell adhesion molecule perturbations: a time-lapse study of the living retina. Mol Cell Neurosci *6*, 433-449. 10.1006/mcne.1995.1032

Cellerino, A., Carroll, P., Thoenen, H., and Barde, Y.A. (1997). Reduced size of retinal ganglion cell axons and hypomyelination in mice lacking brain-derived neurotrophic factor. Mol Cell Neurosci *9*, 397-408. 10.1006/mcne.1997.0641

Chai, L., and Morris, J.E. (1999). Heparan sulfate in the inner limiting membrane of embryonic chicken retina binds basic fibroblast growth factor to promote axonal outgrowth. Exp Neurol *160*, 175-185. 10.1006/exnr.1999.7195

Chan, Y.M., Keramaris-Vrantsis, E., Lidov, H.G., Norton, J.H., Zinchenko, N., Gruber, H.E., Thresher, R., Blake, D.J., Ashar, J., Rosenfeld, J., *et al.* (2010). Fukutin-related protein is essential for mouse muscle, brain and eye development and mutation recapitulates the wide clinical spectrums of dystroglycanopathies. Hum Mol Genet *19*, 3995-4006. 10.1093/hmg/ddq314

Deiner, M.S., Kennedy, T.E., Fazeli, A., Serafini, T., Tessier-Lavigne, M., and Sretavan, D.W. (1997). Netrin-1 and DCC mediate axon guidance locally at the optic disc: loss of function leads to optic nerve hypoplasia. Neuron *19*, 575-589

Dobyns, W.B., Pagon, R.A., Armstrong, D., Curry, C.J., Greenberg, F., Grix, A., Holmes, L.B., Laxova, R., Michels, V.V., Robinow, M., *et al.* (1989). Diagnostic criteria for Walker-Warburg syndrome. Am J Med Genet *32*, 195-210. 10.1002/ajmg.1320320213

Edwards, M.M., Mammadova-Bach, E., Alpy, F., Klein, A., Hicks, W.L., Roux, M., Simon-Assmann, P., Smith, R.S., Orend, G., Wu, J., *et al.* (2010). Mutations in Lama1 disrupt retinal vascular development and inner limiting membrane formation. J Biol Chem *285*, 7697-7711. PMC2844215. 10.1074/jbc.M109.069575

Ford, K.J., Felix, A.L., and Feller, M.B. (2012). Cellular mechanisms underlying spatiotemporal features of cholinergic retinal waves. The Journal of Neuroscience *32*, 850-863. PMC3311224. 10.1523/JNEUROSCI.5309-12.2012

Fruh, S., Romanos, J., Panzanelli, P., Burgisser, D., Tyagarajan, S.K., Campbell, K.P., Santello, M., and Fritschy, J.M. (2016). Neuronal Dystroglycan Is Necessary for Formation and Maintenance of Functional CCK-Positive Basket Cell Terminals on Pyramidal Cells. The Journal of Neuroscience *36*, 10296-10313. 10.1523/jneurosci.1823-16.2016

Fruttiger, M. (2007). Development of the retinal vasculature. Angiogenesis *10*, 77-88. 10.1007/s10456-007-9065-1

Fuerst, P.G., Koizumi, A., Masland, R.H., and Burgess, R.W. (2008). Neurite arborization and mosaic spacing in the mouse retina require DSCAM. Nature *451*, 470-474. PMC2259282. 10.1038/nature06514

Furuta, Y., Lagutin, O., Hogan, B.L., and Oliver, G.C. (2000). Retina- and ventral forebrain-specific Cre recombinase activity in transgenic mice. Genesis *26*, 130-132

Galli-Resta, L., Novelli, E., and Viegi, A. (2002). Dynamic microtubule-dependent interactions position homotypic neurones in regular monolayered arrays during retinal development. Development *129*, 3803-3814

Galli-Resta, L., Resta, G., Tan, S.S., and Reese, B.E. (1997). Mosaics of islet-1-expressing amacrine cells assembled by short-range cellular interactions. The Journal of Neuroscience *17*, 7831-7838

Gnanaguru, G., Bachay, G., Biswas, S., Pinzon-Duarte, G., Hunter, D.D., and Brunken, W.J. (2013). Laminins containing the beta2 and gamma3 chains regulate astrocyte migration and angiogenesis in the retina. Development *140*, 2050-2060. PMC3631977. 10.1242/dev.087817

Godfrey, C., Foley, A.R., Clement, E., and Muntoni, F. (2011). Dystroglycanopathies: coming into focus. Current Opinion in Genetics & Development *21*, 278-285. 10.1016/j.gde.2011.02.001

Halfter, W., Reckhaus, W., and Kroger, S. (1987). Nondirected axonal growth on basal lamina from avian embryonic neural retina. The Journal of Neuroscience *7*, 3712-3722

Halfter, W., Willem, M., and Mayer, U. (2005). Basement membrane-dependent survival of retinal ganglion cells. Invest Ophthalmol Vis Sci *46*, 1000-1009. 10.1167/iovs.04-1185

Huckfeldt, R.M., Schubert, T., Morgan, J.L., Godinho, L., Di Cristo, G., Huang, Z.J., and Wong, R.O.L. (2009). Transient neurites of retinal horizontal cells exhibit columnar tiling via homotypic interactions. Nature Neuroscience *12*, 35-43. 10.1038/nn.2236

Icha, J., Kunath, C., Rocha-Martins, M., and Norden, C. (2016). Independent modes of ganglion cell translocation ensure correct lamination of the zebrafish retina. J Cell Biol *215*, 259-275. PMC5084647. 10.1083/jcb.201604095

Kay, J.N., Chu, M.W., and Sanes, J.R. (2012). MEGF10 and MEGF11 mediate homotypic interactions required for mosaic spacing of retinal neurons. Nature *483*, 465-469. PMC3310952. 10.1038/nature10877

Kay, J.N., Roeser, T., Mumm, J.S., Godinho, L., Mrejeru, A., Wong, R.O.L., and Baier, H. (2004). Transient requirement for ganglion cells during assembly of retinal synaptic layers. Development *131*, 1331-1342. 10.1242/dev.01040

Lee, Y., Kameya, S., Cox, G.A., Hsu, J., Hicks, W., Maddatu, T.P., Smith, R.S., Naggert, J.K., Peachey, N.S., and Nishina, P.M. (2005). Ocular abnormalities in Large(myd) and Large(vls) mice, spontaneous models for muscle, eye, and brain diseases. Mol Cell Neurosci *30*, 160-172. 10.1016/j.mcn.2005.07.009

Li, S., Sukeena, J.M., Simmons, a.B., Hansen, E.J., Nuhn, R.E., Samuels, I.S., and Fuerst, P.G. (2015). DSCAM Promotes Refinement in the Mouse Retina through Cell Death and Restriction of Exploring Dendrites. Journal of Neuroscience *35*, 5640-5654. 10.1523/JNEUROSCI.2202-14.2015

Livesey, F.J., and Cepko, C.L. (2001). Vertebrate neural cell-fate determination: lessons from the retina. Nature Reviews Neuroscience *2*, 109-118. 10.1038/35053522

Marcos, S., Nieto-Lopez, F., Sandonìs, A., Cardozo, M.J., Marco, F.D., Esteve, P., and Bovolenta, P. (2015). Secreted frizzled related proteins modulate pathfinding and fasciculation of

mouse retina ganglion cell axons by direct and indirect mechanisms. The Journal Neuroscience *35*, 4729-4740. 10.1523/JNEUROSCI.3304-13.2015

Montanaro, F., Carbonetto, S., Campbell, K.P., and Lindenbaum, M. (1995). Dystroglycan expression in the wild type and mdx mouse neural retina: synaptic colocalization with dystrophin, dystrophin-related protein but not laminin. Journal of Neuroscience Research *42*, 528-538. 10.1002/jnr.490420411

Moore, C.J., and Winder, S.J. (2010). Dystroglycan versatility in cell adhesion: a tale of multiple motifs. Cell Communication and Signaling *8*, 3. 10.1186/1478-811X-8-3

Moore, C.J., and Winder, S.J. (2012). The inside and out of dystroglycan post-translational modification. Neuromuscular Disorders *22*, 959-965. 10.1016/j.nmd.2012.05.016

Moore, S.A., Saito, F., Chen, J., Michele, D.E., Henry, M.D., Messing, A., Cohn, R.D., Ross-Barta, S.E., Westra, S., Williamson, R.A.*, et al.* (2002). Deletion of brain dystroglycan recapitulates aspects of congenital muscular dystrophy. Nature *418*, 422-425. 10.1038/nature00838

Morgan, J., and Wong, R. (1995). Development of Cell Types and Synaptic Connections in the Retina. In Webvision: The Organization of the Retina and Visual System, H. Kolb, E. Fernandez, and R. Nelson, eds. (Salt Lake City (UT)).

Myshrall, T.D., Moore, S.A., Ostendorf, A.P., Satz, J.S., Kowalczyk, T., Nguyen, H., Daza, R.A., Lau, C., Campbell, K.P., and Hevner, R.F. (2012). Dystroglycan on radial glia end feet is required for pial basement membrane integrity and columnar organization of the developing cerebral cortex. J Neuropathol Exp Neurol *71*, 1047-1063. PMC3512206. 10.1097/NEN.0b013e318274a128

Nakagawa, N., Yagi, H., Kato, K., Takematsu, H., and Oka, S. (2015). Ectopic clustering of Cajal-Retzius and subplate cells is an initial pathological feature in Pomgnt2-knockout mice, a model of dystroglycanopathy. Scientific Reports *5*, 11163. PMC4461912. 10.1038/srep11163

Omori, Y., Araki, F., Chaya, T., Kajimura, N., Irie, S., Terada, K., Muranishi, Y., Tsujii, T., Ueno, S., Koyasu, T.*, et al.* (2012). Presynaptic dystroglycan-pikachurin complex regulates the proper synaptic connection between retinal photoreceptor and bipolar cells. The Journal Neuroscience *32*, 6126-6137. 10.1523/JNEUROSCI.0322-12.2012

Ott, H., Bastmeyer, M., and Stuermer, C.A. (1998). Neurolin, the goldfish homolog of DM-GRASP, is involved in retinal axon pathfinding to the optic disk. The Journal of Neuroscience *18*, 3363-3372

Pan, L., Deng, M., Xie, X., and Gan, L. (2008). ISL1 and BRN3B co-regulate the differentiation of murine retinal ganglion cells. Development *135*, 1981-1990. 10.1242/dev.010751

Petros, T.J., Rebsam, A., and Mason, C.A. (2008). Retinal axon growth at the optic chiasm: to cross or not to cross. Annual Review of Neuroscience *31*, 295-315. 10.1146/annurev.neuro.31.060407.125609

Pinzon-Duarte, G., Daly, G., Li, Y.N., Koch, M., and Brunken, W.J. (2010). Defective formation of the inner limiting membrane in laminin beta2- and gamma3-null mice produces retinal dysplasia. Invest Ophthalmol Vis Sci *51*, 1773-1782. PMC2868416. 10.1167/iovs.09-4645

Randlett, O., Poggi, L., Zolessi, F.R., and Harris, W.A. (2011). The oriented emergence of axons from retinal ganglion cells is directed by laminin contact in vivo. Neuron *70*, 266-280. 10.1016/j.neuron.2011.03.013

Reese, B.E. (2011). Development of the retina and optic pathway. Vision research *51*, 613-632. 10.1016/j.visres.2010.07.010

Reese, B.E., Necessary, B.D., Tam, P.P., Faulkner-Jones, B., and Tan, S.S. (1999). Clonal expansion and cell dispersion in the developing mouse retina. Eur J Neurosci *11*, 2965-2978

Riccomagno, M.M., Sun, L.O., Brady, C.M., Alexandropoulos, K., Seo, S., Kurokawa, M., and Kolodkin, A.L. (2014). Cas adaptor proteins organize the retinal ganglion cell layer downstream of integrin signaling. Neuron *81*, 779-786. 10.1016/j.neuron.2014.01.036

Rohrer, B., LaVail, M.M., Jones, K.R., and Reichardt, L.F. (2001). Neurotrophin receptor TrkB activation is not required for the postnatal survival of retinal ganglion cells in vivo. Exp Neurol *172*, 81-91. 10.1006/exnr.2001.7795

Sato, S., Omori, Y., Katoh, K., Kondo, M., Kanagawa, M., Miyata, K., Funabiki, K., Koyasu, T., Kajimura, N., Miyoshi, T.*, et al.* (2008). Pikachurin, a dystroglycan ligand, is essential for photoreceptor ribbon synapse formation. Nature Neuroscience *11*, 923-931. 10.1038/nn.2160

Satz, J.S., Barresi, R., Durbeej, M., Willer, T., Turner, A., Moore, S.A., and Campbell, K.P. (2008). Brain and eye malformations resembling Walker-Warburg syndrome are recapitulated in mice by dystroglycan deletion in the epiblast. The Journal of Neuroscience *28*, 10567-10575. 10.1523/JNEUROSCI.2457-08.2008

Satz, J.S., Ostendorf, A.P., Hou, S., Turner, A., Kusano, H., Lee, J.C., Turk, R., Nguyen, H., Ross-Barta, S.E., Westra, S.*, et al.* (2010). Distinct functions of glial and neuronal dystroglycan in the developing and adult mouse brain. The Journal of Neuroscience *30*, 14560-14572. 10.1523/JNEUROSCI.3247-10.2010

Satz, J.S., Philp, A.R., Nguyen, H., Kusano, H., Lee, J., Turk, R., Riker, M.J., Hernández, J., Weiss, R.M., Anderson, M.G.*, et al.* (2009). Visual impairment in the absence of dystroglycan. The Journal of Neuroscience *29*, 13136-13146. 10.1523/JNEUROSCI.0474-09.2009

Takahashi, H., Kanesaki, H., Igarashi, T., Kameya, S., Yamaki, K., Mizota, A., Kudo, A., Miyagoe-Suzuki, Y., Takeda, S., and Takahashi, H. (2011). Reactive gliosis of astrocytes and Muller glial cells in retina of POMGnT1-deficient mice. Mol Cell Neurosci *47*, 119-130. 10.1016/j.mcn.2011.03.006

Takeda, S., Kondo, M., Sasaki, J., Kurahashi, H., Kano, H., Arai, K., Misaki, K., Fukui, T., Kobayashi, K., Tachikawa, M.*, et al.* (2003). Fukutin is required for maintenance of muscle integrity, cortical histiogenesis and normal eye development. Hum Mol Genet *12*, 1449-1459

Taniguchi-Ikeda, M., Morioka, I., Iijima, K., and Toda, T. (2016). Mechanistic aspects of the formation of alpha-dystroglycan and therapeutic research for the treatment of alpha-dystroglycanopathy: A review. Mol Aspects Med *51*, 115-124. 10.1016/j.mam.2016.07.003

Tao, C., and Zhang, X. (2016). Retinal Proteoglycans Act as Cellular Receptors for Basement Membrane Assembly to Control Astrocyte Migration and Angiogenesis. Cell Rep *17*, 1832-1844. PMC5129871. 10.1016/j.celrep.2016.10.035

Taylor, L., Arner, K., Engelsberg, K., and Ghosh, F. (2015). Scaffolding the retina: the interstitial extracellular matrix during rat retinal development. Int J Dev Neurosci *42*, 46-58. 10.1016/j.ijdevneu.2015.03.002

Thompson, H., Camand, O., Barker, D., and Erskine, L. (2006). Slit proteins regulate distinct aspects of retinal ganglion cell axon guidance within dorsal and ventral retina. The Journal of Neuroscience *26*, 8082-8091. 10.1523/JNEUROSCI.1342-06.2006

Tronche, F., Kellendonk, C., Kretz, O., Gass, P., Anlag, K., Orban, P.C., Bock, R., Klein, R., and Schutz, G. (1999). Disruption of the glucocorticoid receptor gene in the nervous system results in reduced anxiety. Nat Genet *23*, 99-103. 10.1038/12703

Varshney, S., Hunter, D.D., and Brunken, W.J. (2015). Extracellular Matrix Components Regulate Cellular Polarity and Tissue Structure in the Developing and Mature Retina. J Ophthalmic Vis Res *10*, 329-339. PMC4687269. 10.4103/2008-322X.170354

Wang, S.W., Kim, B.S., Ding, K., Wang, H., Sun, D., Johnson, R.L., Klein, W.H., and Gan, L. (2001). Requirement for math5 in the development of retinal ganglion cells. Genes Dev *15*, 24-29. PMC312600

Wassle, H., and Riemann, H.J. (1978). The mosaic of nerve cells in the mammalian retina. Proc R Soc Lond B Biol Sci *200*, 441-461

Wright, K.M., Lyon, K.A., Leung, H., Leahy, D.J., Ma, L., and Ginty, D.D. (2012). Dystroglycan organizes axon guidance cue localization and axonal pathfinding. Neuron *76*, 931-944. 10.1016/j.neuron.2012.10.009

Xiao, T., Staub, W., Robles, E., Gosse, N.J., Cole, G.J., and Baier, H. (2011). Assembly of lamina-specific neuronal connections by slit bound to type IV collagen. Cell *146*, 164-176. PMC3136219. 10.1016/j.cell.2011.06.016

Xu, H.P., Burbridge, T.J., Ye, M., Chen, M., Ge, X., Zhou, Z.J., and Crair, M.C. (2016). Retinal Wave Patterns Are Governed by Mutual Excitation among Starburst Amacrine Cells and Drive the Refinement and Maintenance of Visual Circuits. The Journal of Neuroscience *36*, 3871-3886. PMC4812142. 10.1523/JNEUROSCI.3549-15.2016

Yang, L., Cai, C.L., Lin, L., Qyang, Y., Chung, C., Monteiro, R.M., Mummery, C.L., Fishman, G.I., Cogen, A., and Evans, S. (2006). Isl1Cre reveals a common Bmp pathway in heart and limb development. Development *133*, 1575-1585. 10.1242/dev.02322

Young, R.W. (1984). Cell death during differentiation of the retina in the mouse. J Comp Neurol *229*, 362-373. 10.1002/cne.902290307

Yurchenco, P.D. (2011). Basement membranes: cell scaffoldings and signaling platforms. Cold Spring Harb Perspect Biol *3*. PMC3039528. 10.1101/cshperspect.a004911

Figure 1

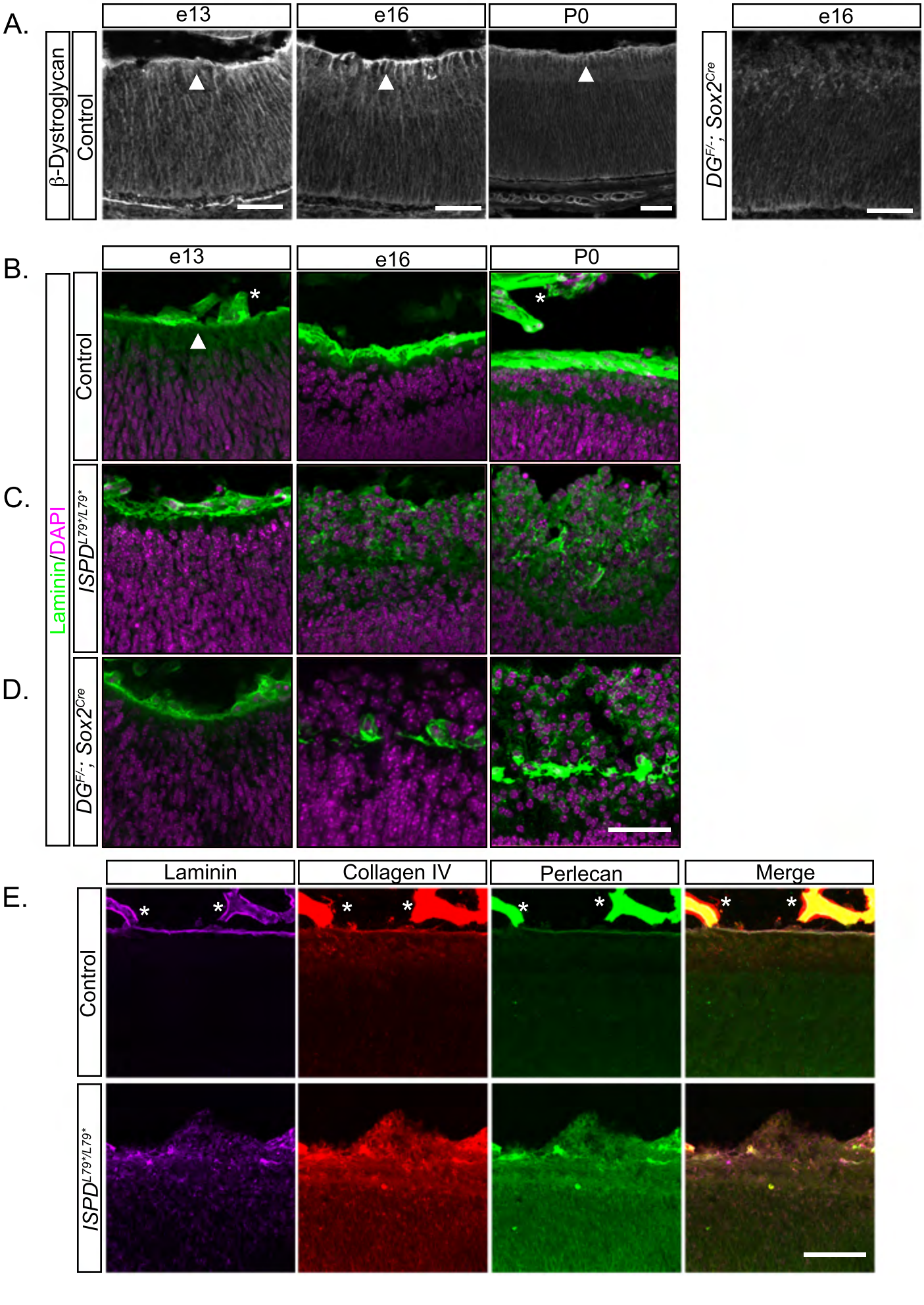

Figure 2

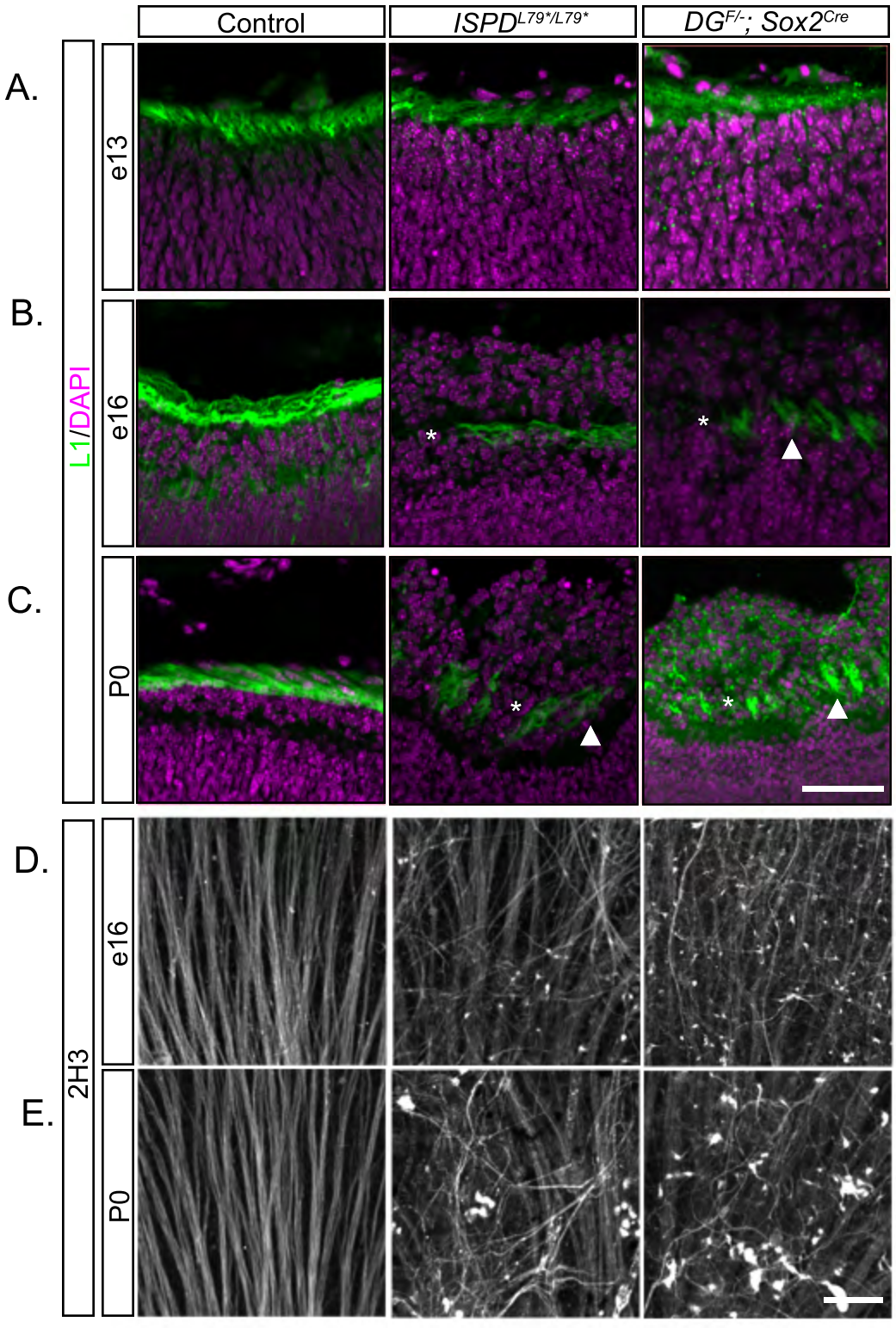

Figure 3

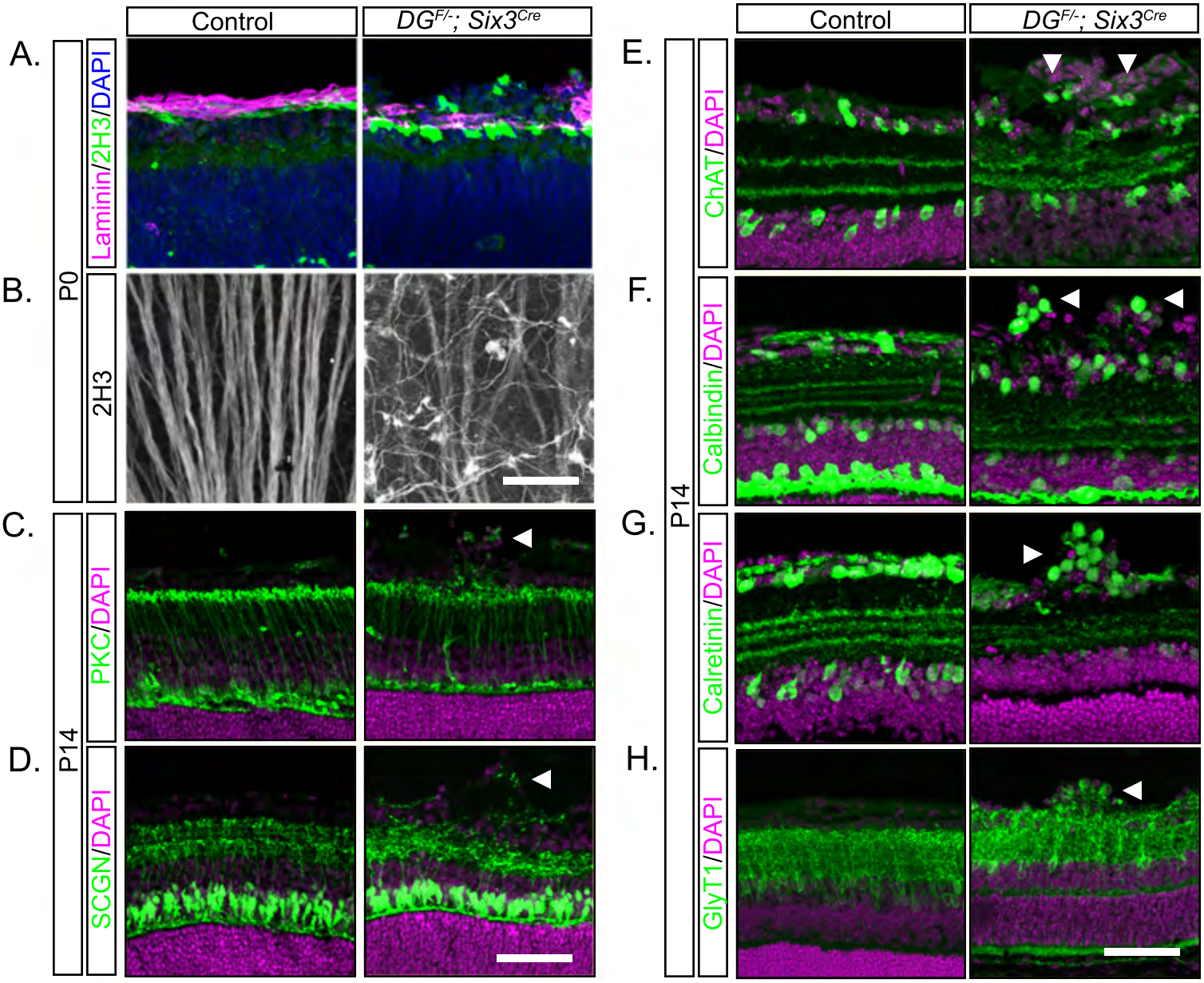

Figure 4

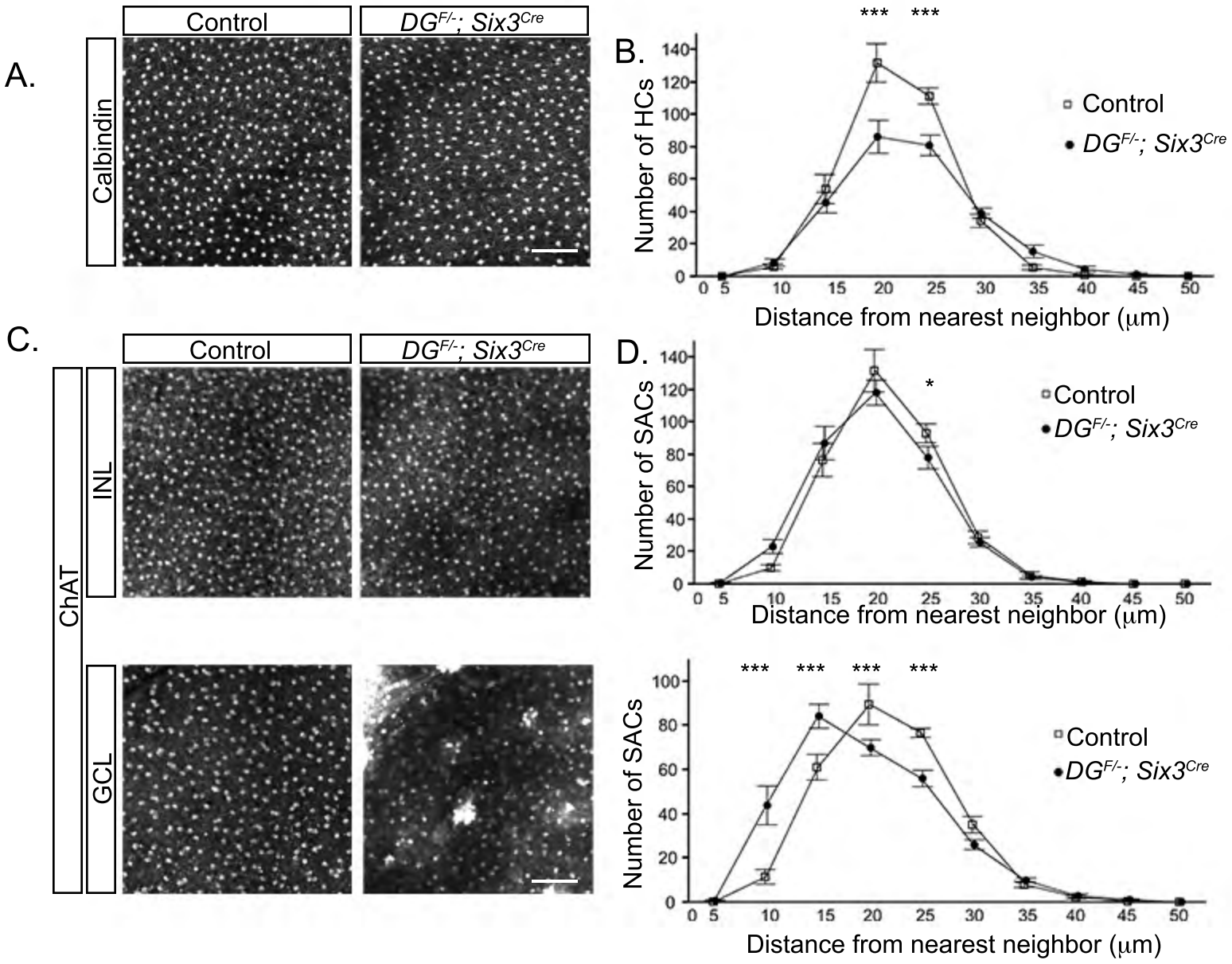

Figure 5

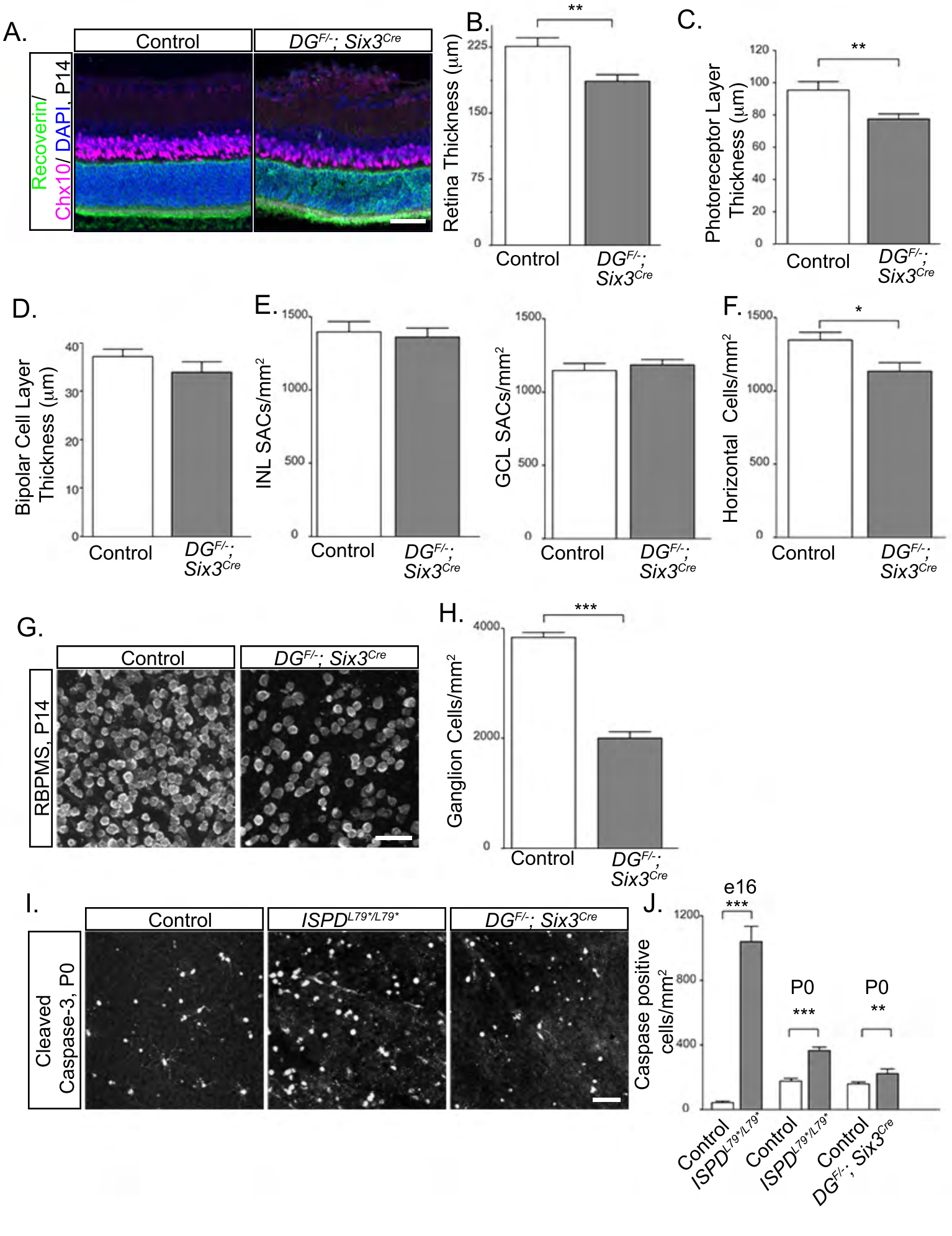

Figure 6

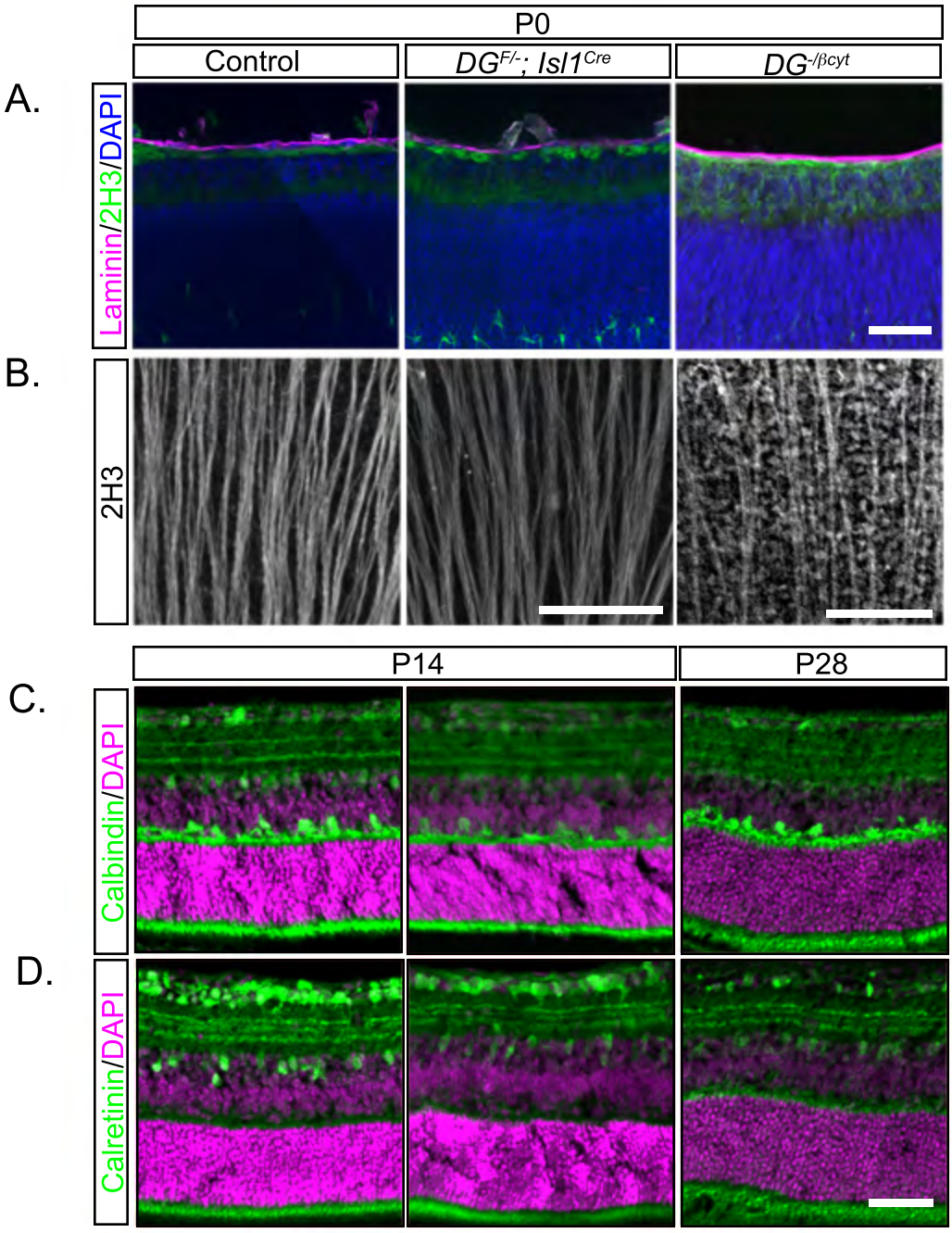

Figure 7

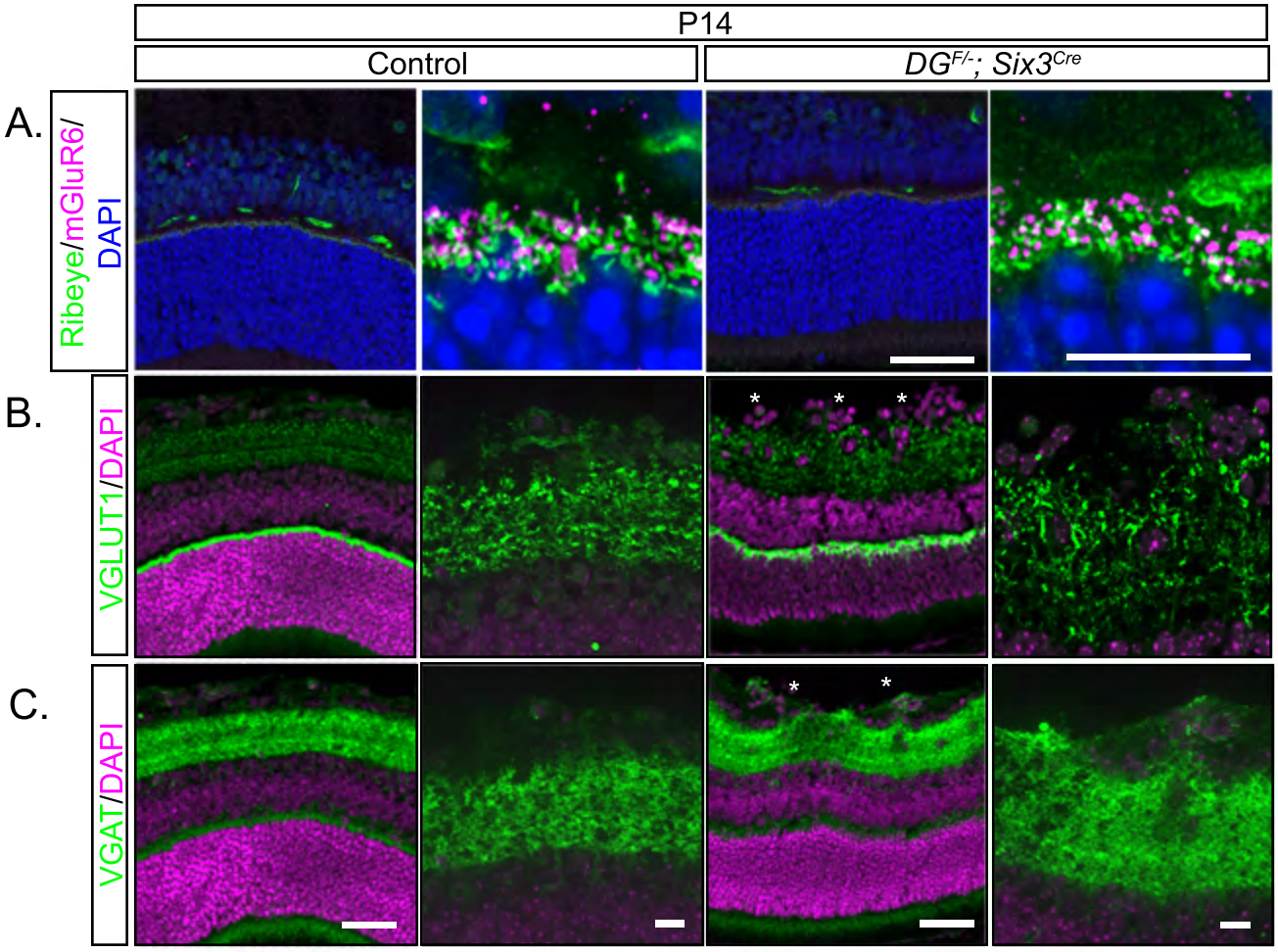

Figure 8

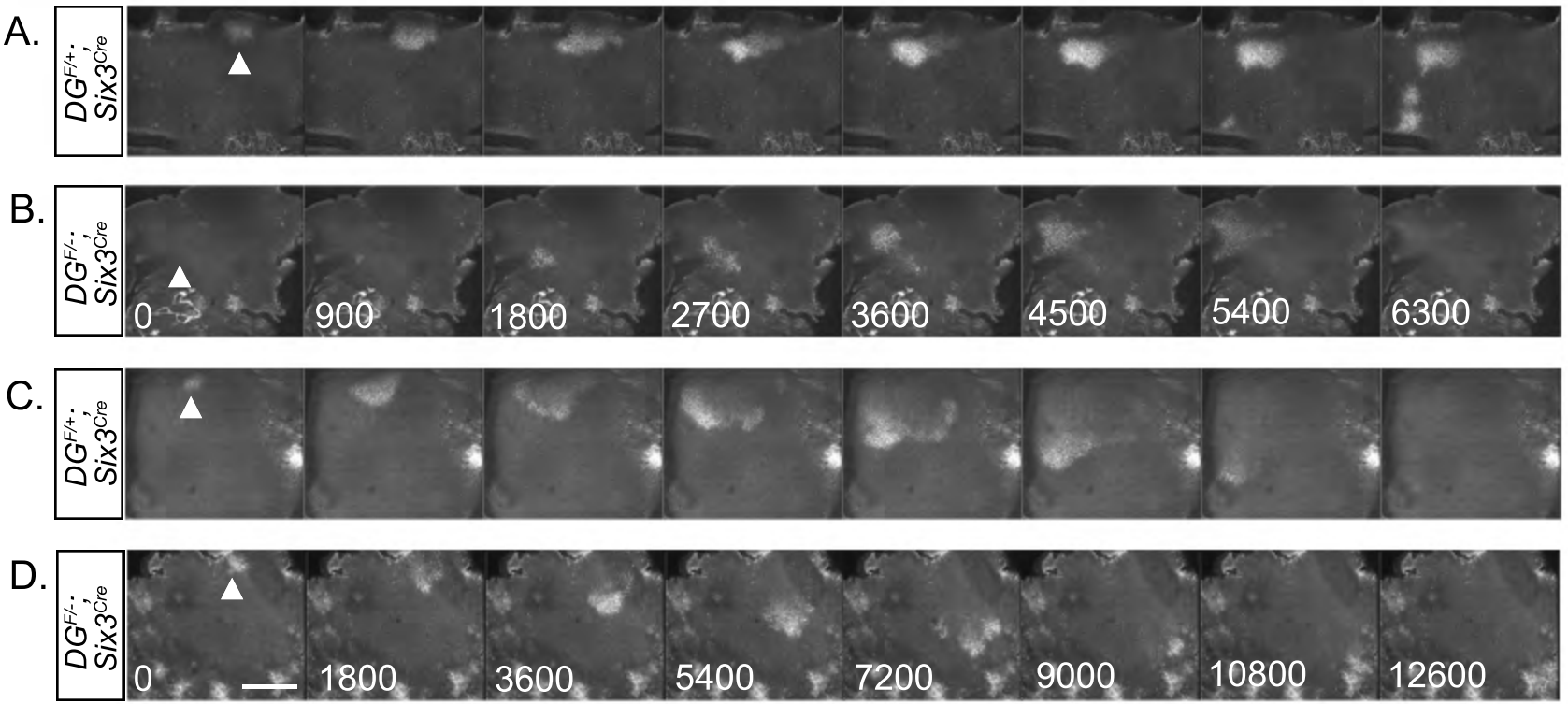
A.
DG^F/+; Six3^Cre
B.
DG^F/-; Six3^Cre
0
900
1800
2700
3600
4500
5400
6300
C.
DG^F/+; Six3^Cre
D.
DG^F/-; Six3^Cre
0
1800
3600
5400
7200
9000
10800
12600

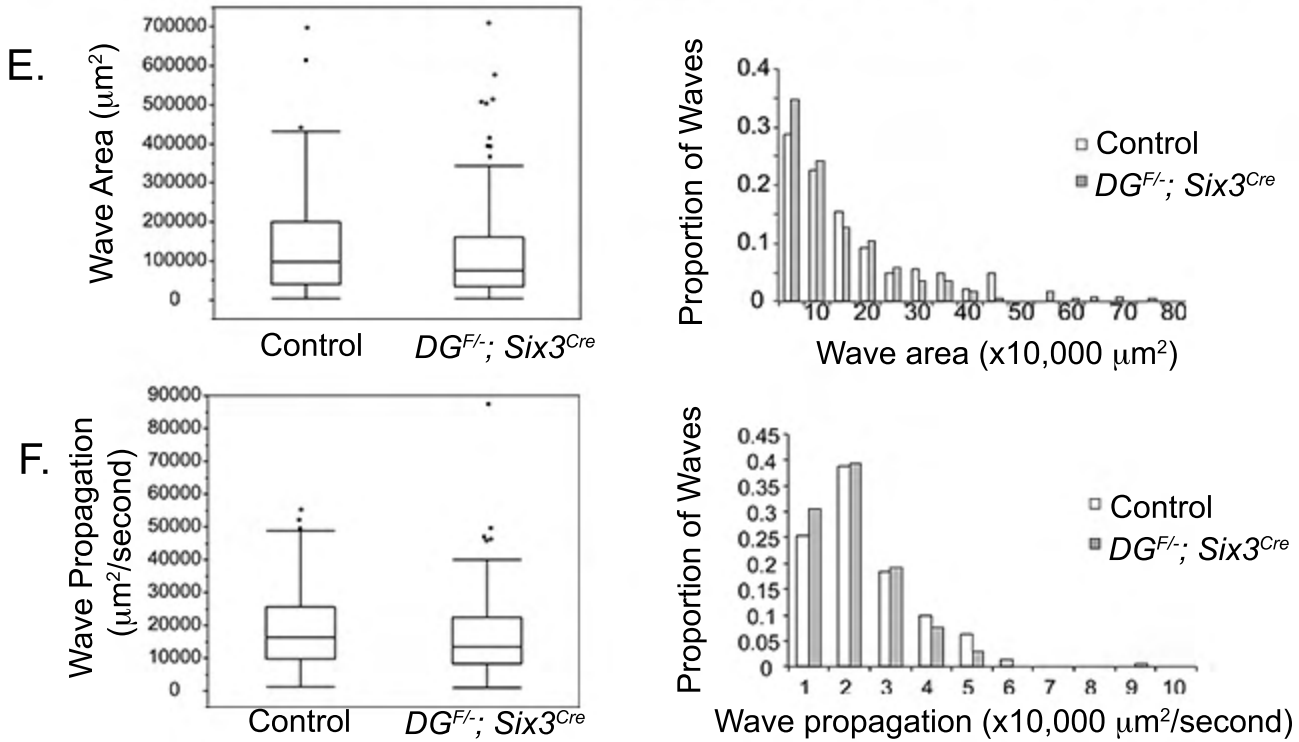
E.
Wave Area (μm²)
700000
600000
500000
400000
300000
200000
100000
0
Control
DG^F/-; Six3^Cre
Proportion of Waves
0.4
0.3
0.2
0.1
0
10 20 30 40 50 60 70 80
Wave area (x10,000 μm²)
Control
DG^F/-; Six3^Cre
F.
Wave Propagation (μm²/second)
90000
80000
70000
60000
50000
40000
30000
20000
10000
0
Control
DG^F/-; Six3^Cre
Proportion of Waves
0.45
0.4
0.35
0.3
0.25
0.2
0.15
0.1
0.05
0
1 2 3 4 5 6 7 8 9 10
Wave propagation (x10,000 μm²/second)
Control
DG^F/-; Six3^Cre

Supplemental Table 1

Target	Host species	Dilution	Company/origin	Catalog #	RRID
Beta DG	rabbit	1:100	Santa Cruz Biotech	sc-28535	AB_782259
Laminin	rabbit	1:1000	Sigma	L9393	AB_477163
Collagen IV	goat	1:250	Southern Biotech	1340-01	AB_2082646
Perlecan	rat	1:500	Millipore	MAB1948P	AB_10615958
L1	rat	1:500	Millipore	MAB5272	AB_2133200
2H3	mouse	1:1000	DSHB	2h3	AB_531793
ChAT	goat	1:500	Millipore	AB144P-200UL	AB_11214092
Calbindin	rabbit	1:10,000	Swant	CB 38	AB_10000340
Calretinin	rabbit	1:10,000	Swant	CG 1	AB_2619710
GlyT1	rabbit	1:800	gift from Dr. David Pow		
PKC	mouse	1:500	Sigma	P5704	AB_477375
Secretagogin	rabbit	1:4000	Biovendor	rd181120100	AB_2034060
Recoverin	rabbit	1:200	Millipore	AB5585	AB_2253622
Chx10	goat	1:500	Santa Cruz Biotech	sc-21690	AB_2216006
RBPMS	guinea pig	1:500	PhosphoSolutions	1832-RBPMS	AB_2492226
Cleaved Caspase-3	rabbit	1:500	Cell Signaling	9661S	AB_2341188
Ribeye/Ctbp2	mouse	1:1000	BD Biosciences	612044	AB_399431
MGluR6	sheep	1:100	gift from Dr. Catherine Morgans		
VGLUT1	guinea pig	1:500	Millipore	AB5905	AB_2301751
VGAT	rabbit	1:500	Synaptic Systems	131-003	AB_887869

Supplemental Figure 1

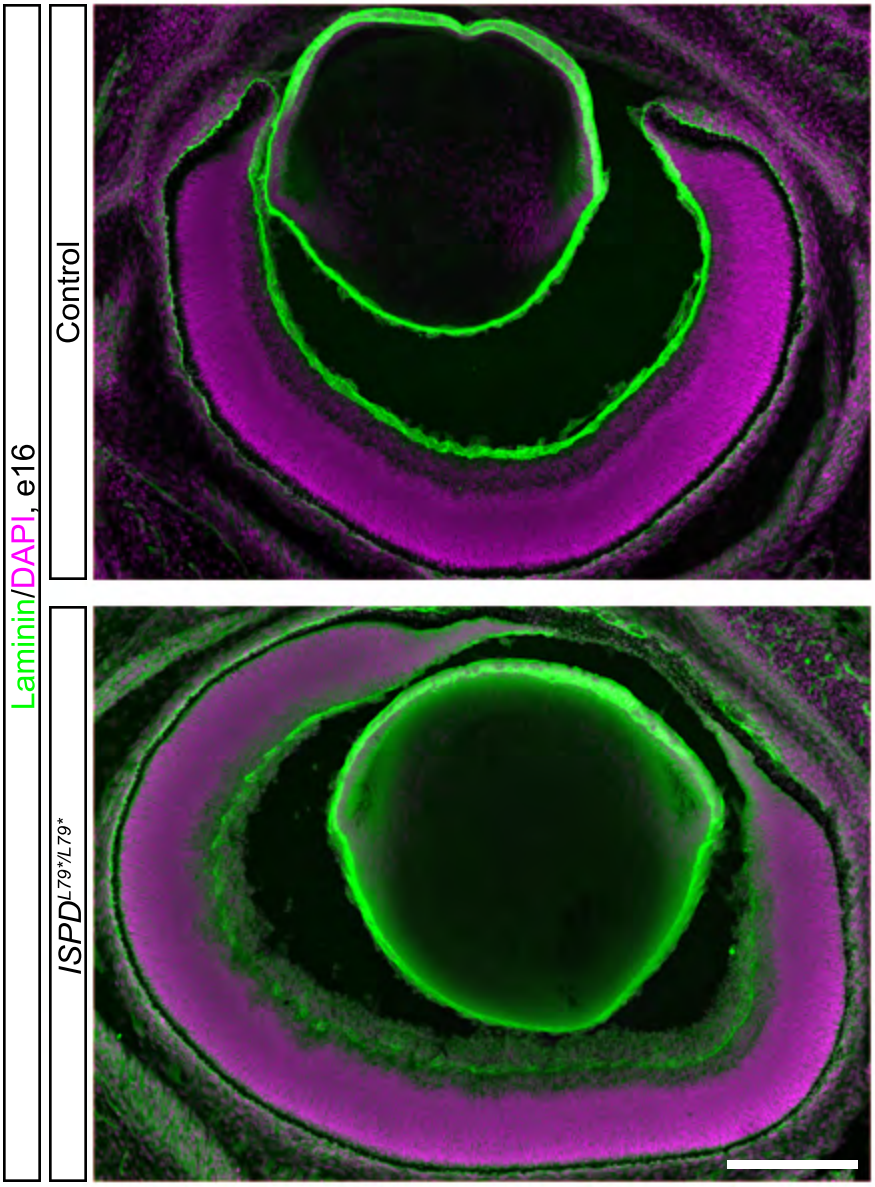

Supplemental Figure 2

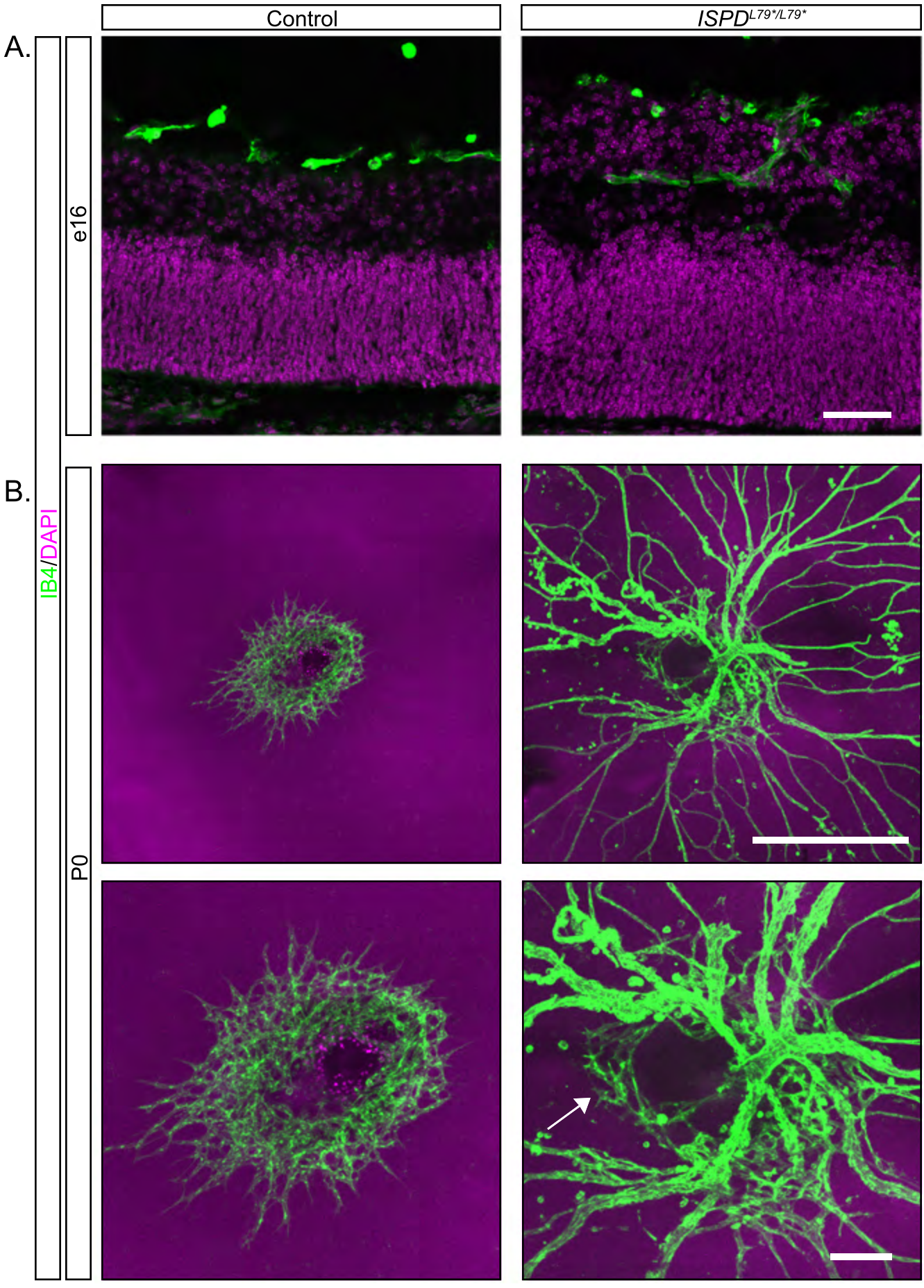

Supplemental Figure 3

A.

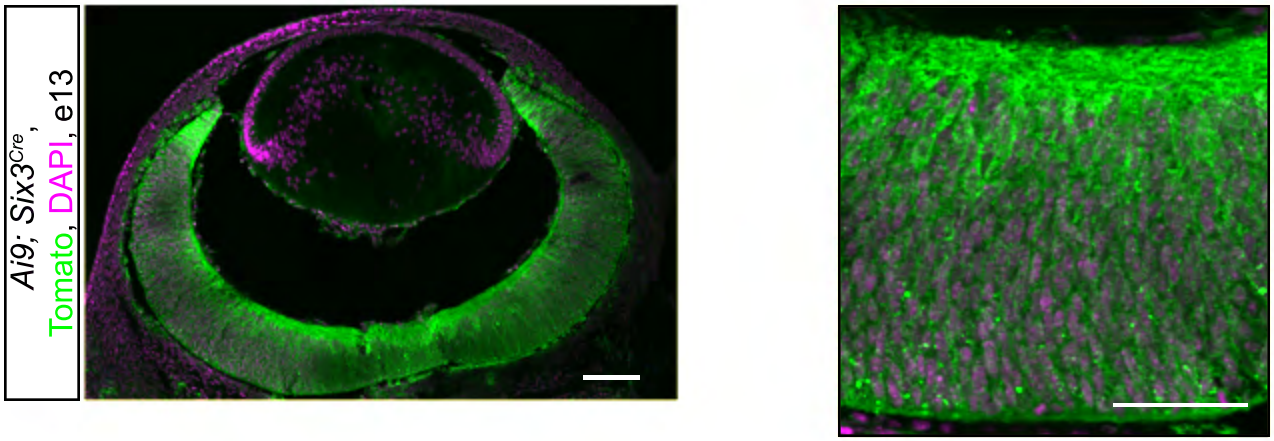

B.

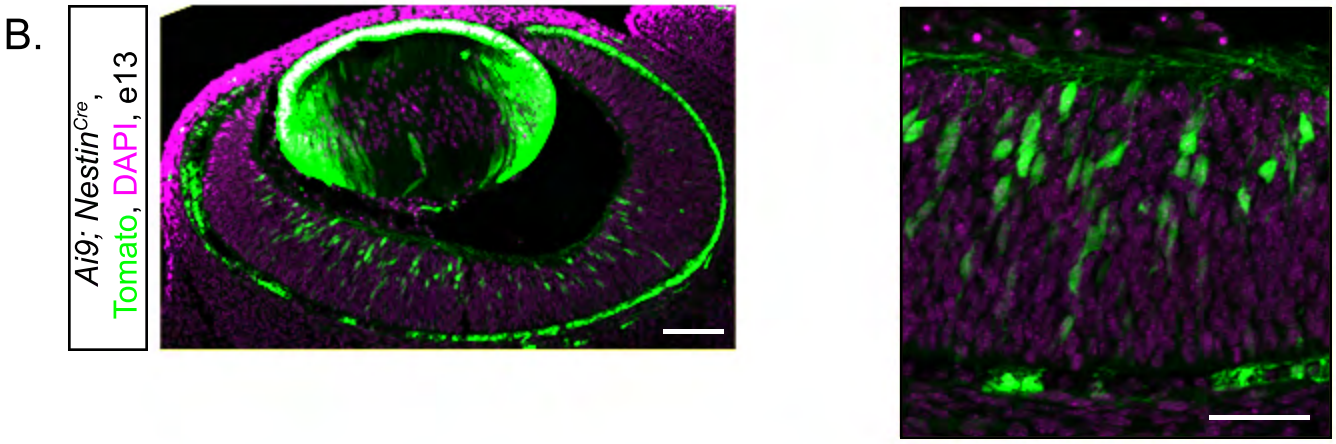

C.

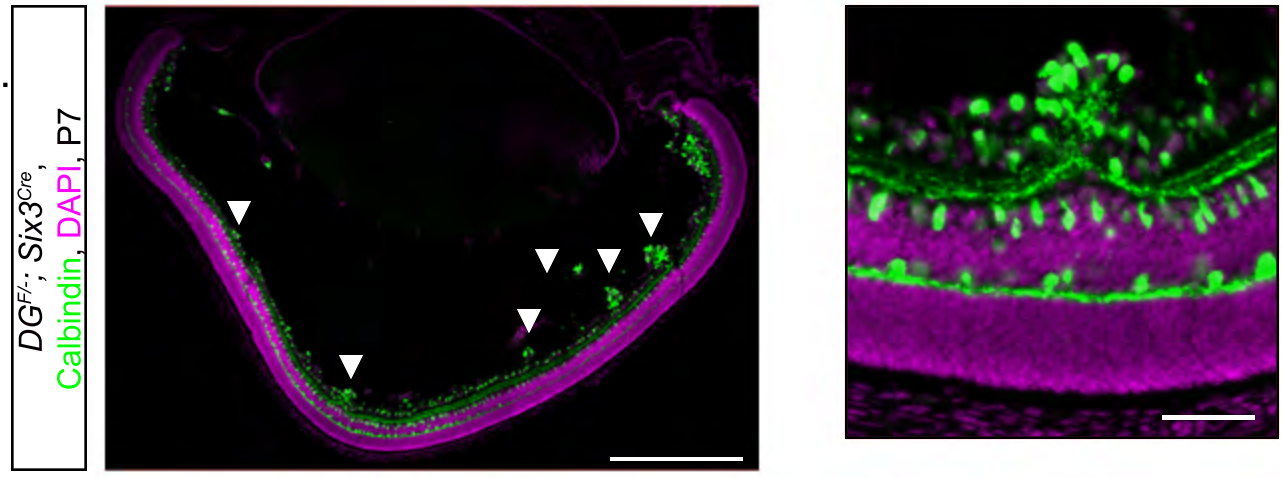

Supplemental Figure 4

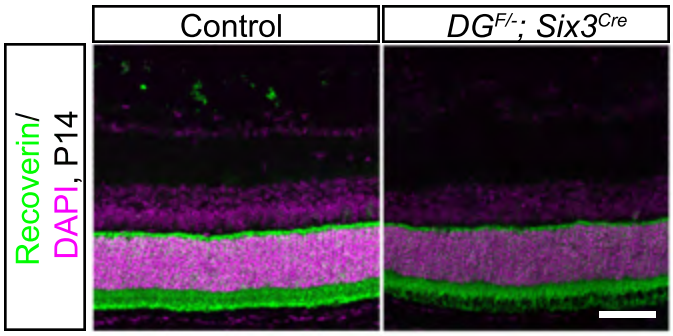

Supplemental Figure 5

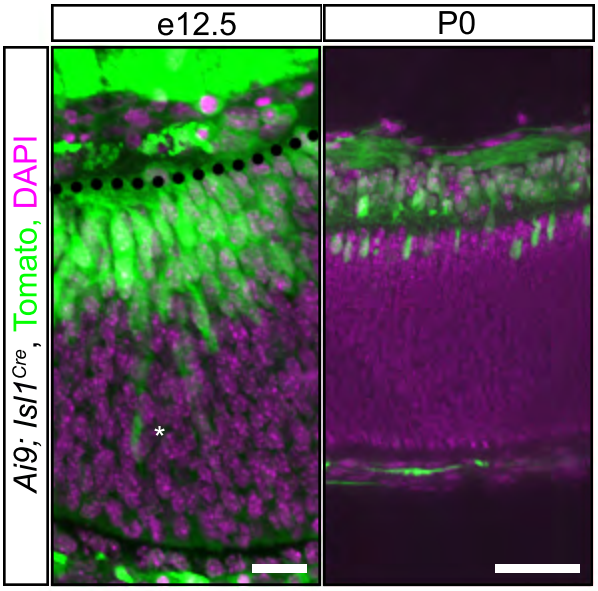

Figure Legends

Figure 1: The inner limiting membrane undergoes progressive degeneration in the absence of functional dystroglycan. (A) Dystroglycan (β-DG) is expressed throughout the developing retina, with an enrichment at the inner limiting membrane (ILM). Dystroglycan expression is lost in $DG^{F/-}$;$Sox2^{Cre}$ mice (right). (B-D) The initial assembly of the ILM occurs normally in the absence of functional dystroglycan in (C) $ISPD^{L79*/L79*}$ and (D) $DG^{F/-}$; $Sox2^{cre}$ retinas. The ILM in $ISPD^{L79*/L79*}$ and $DG^{F/-}$; $Sox2^{cre}$ retinas undergoes progressive degeneration at e16 (middle) and P0 (right), and retinal neurons migrate into the vitreous. (E) Localization of multiple extracellular matrix proteins, including laminin (purple), collagen IV (red), and perlecan (green), is disrupted in the ILM in the absence of functional dystroglycan in $ISPD^{L79*/L79*}$ retinas at P0. Arrowheads indicate ILM, asterisks indicate blood vessels. Scale bar, 50μm.

Figure 2: Dystroglycan is required for intraretinal axon guidance (A) L1 positive axons in the optic fiber layer (OFL) initially appear normal in $ISPD^{L79*/L79*}$ (middle), and $DG^{F/-}$; $Sox2^{cre}$ retinas (right) at e13. (B, C) As the ILM degenerates in $ISPD^{L79*/L79*}$ and $DG^{F/-}$; $Sox2^{cre}$ retinas at e16 (B) and P0 (C), axons hyperfasciculate (arrowhead) and exhibit gaps (asterisk) within the OFL. (D, E). Flat mount preparations from $ISPD^{L79*/L79*}$ and $DG^{F/-}$; $Sox2^{cre}$ retinas at e16 (D) and P0 (E) show progressive disruption of axon tracts (Neurofilament, 2H3). Scale bar, 50 μm.

Figure 3: Disrupted circuit formation in the inner retina of postnatal *dystroglycan* mutants. (A, B) $DG^{F/-}$; $Six3^{cre}$ (right) mice exhibit inner limiting membrane degeneration (top, purple, laminin) and abnormal axonal fasciculation and guidance (top, green, bottom, 2H3). (C-D) The cell bodies of bipolar cells (PKC, C, SCGN, D) exhibit normal lamination patters, while their axons extend into ectopic cellular clusters in the ganglion cell layer. (E-H) Abnormal cellular lamination and disruptions in dendritic stratification of multiple amacrine and retinal ganglion cell types is observed in $DG^{F/-}$; $Six3^{cre}$ retinas. (E) ChAT labels starburst amacrine cells, (F) calbindin and (G) calretinin label amacrine and ganglion cells, and (H) GlyT1 labels glycinergic amacrine cells. Arrowheads indicate axons or cell bodies in ectopic clusters. Scale bar, 50 μm.

Figure 4: Dystroglycan is required for mosaic cell spacing in the ganglion cell layer. (A, B). Horizontal cells (2H3) in flat mount P14 adult retinas have reduced cellular density, but normal mosaic cell spacing curves (Nearest neighbor analysis, Two-Way ANOVA, n=20 samples from 5 control retinas, 18 samples from 5 mutant retinas). (C, D) Mosaic cell spacing of starburst amacrine cells (ChAT) in the inner nuclear layer is normal (Nearest neighbor analysis, Two-Way ANOVA, n=10 samples from 3 control retinas, 10 samples from 3 mutant retinas), while the ectopic clustering of starburst amacrine cells in the ganglion cell layer results in a significant disruption of mosaic spacing (Nearest

neighbor analysis, Two-Way ANOVA, n=10 samples from 3 control retinas, 10 samples from 3 mutant retinas). Scale bar 100μm.

Figure 5: Retinal thinning in *dystroglycan* mutants. (A-D) P14 *DG$^{F/-}$; Six3^{cre}* retinas show decreased retinal thickness (DAPI, p<0.01, n=7 control, 7 mutant), a decreased thickness of the photoreceptor layer (C, Recoverin, green, p<0.01, n=7 control, 7 mutant) and no change in thickness of the bipolar cell layer (D, Chx10, purple, p>0.05, n=7 control, 7 mutant). Starburst amacrine cell density is normal in both the GCL and INL (E, n=10 samples from 3 control retinas, 10 samples from 3 mutant retinas), while horizontal cells show a slight reduction in cell density (F) in P14 *DG$^{F/-}$; Six3^{cre}* retinas (p<0.05, n=20 samples from 5 control retinas, 18 samples from 5 mutant retinas). (G,H) Ganglion cell density (RBPMS) is reduced by approximately 50% in P14 *DG$^{F/-}$; Six3^{cre}* retinas (p<0.0001, n=12 samples from 3 control retinas, 12 samples from 3 mutant retinas). (I-J) Immunohistochemistry for cleaved caspase-3 in a flat mount preparation of P0 *DG$^{F/-}$; Six3^{cre}* retinas shows an increase in apoptotic cells. (t test, p<0.05, n=18 samples from 6 control retinas, 17 samples from 6 mutant retinas). (J) Quantification of cleaved caspase-3 positive cells shows an increase in apoptotic cells at e16 (t test, p<0.0001, n=18 samples from 6 control retinas, 18 samples from 8 mutant retinas) and P0 (I,J t test, p<0.0001, n=18 samples from 6 control retinas, 15 samples from 5 mutant retinas) between control (left) and *ISPD$^{L79*/L79*}$* (middle) retinas. Scale bar 50 μm.

Figure 6: Dystroglycan functions non-cell autonomously and does not require its intracellular signaling domain for retinal development. (A) The ILM (laminin, purple) and axons in the OFL (2H3, green) appear similar to control in *DG$^{F/-}$; Isl1^{cre}* (middle panel) retinas and mice lacking the intracellular domain of dystroglycan (*DG$^{-/βcyt}$*) (right panel) retinas at P0. (B) Flat mount preparations show normal axon fasciculation (2H3) in *DG$^{F/-}$; Isl1^{cre}* (middle panel) retinas and *DG$^{-/βcyt}$* (right panel) retinas. (C-D) *DG$^{F/-}$; Isl1^{cre}* (middle panel) retinas (P14) and *DG$^{-/βcyt}$* (right panel) retinas (P28) have normal cellular lamination and dendritic stratification. Scale bar, 50 μm.

Figure 7: Dystroglycan is dispensable for synapse formation in the retina. (A) Markers for outer retinal ribbon synapses (Ribeye, presynaptic and mGluR6, postsynaptic) appear structurally normal in the absence of dystroglycan. The density of (B) excitatory (VGLUT1) and (C) inhibitory (VGAT) presynaptic markers appear similar to control in the inner retinas of *DG$^{F/-}$; Six3^{cre}* mutants. Synapses are also present within ectopic clusters (asterisks). Scale bar, 50 μm wide view, scale bar,10 μm enlarged view.

Figure 8: Dystroglycan is dispensable for the generation and propagation of retinal waves. (A-D) At P1, waves propagate normally across the retina in *DG$^{F/+}$; Six3^{cre}; R26-LSL-GCaMP6f* (A, C) and *DG^{F-}; Six3^{cre}; R26-LSL-GCaMP6f* mice (B, D). Both small (A, B) and large (C, D) retinal waves are present at a similar frequency in *DG$^{F/+}$; Six3^{cre}; R26-LSL-GCaMP6f* and *DG$^{F/-}$; Six3^{cre}; R26-*

LSL-GCaMP6f retinas. (E) Distributions of wave areas show no difference between controls and mutants (Wilcoxon rank sum test, $p>0.05$). (F) Wave propagation rate is significantly slower in mutant retinas (Wilcoxon rank sum test, $p<0.05$). Wave parameters were calculated from 142 control waves obtained from 6 retinas from 3 control mice and 173 mutant waves obtained from 8 retinas from 5 mutant mice. Arrowheads indicate the initiation site of a retinal wave. Scale bar 500 μm. Time displayed in milliseconds.

Supplemental Figure Legends

Supplemental Figure 1: Cellular migration defects encompass the entire retina in *ISPD$^{L79*/L79*}$* mutants. The ILM in *ISPD$^{L79*/L79*}$* retinas undergoes degeneration (bottom panel) that is present across the entire span of the retina at e16. Laminin, green, DAPI, purple. Scale bar, 200 μm.

Supplemental Figure 2: Dystroglycan is required for normal vasculature development. (A) IB4 labeled hyaloid vasculature is present in the vitreous adjacent to the GCL in control retinas (left) but is embedded within ectopic cell clusters *ISPD$^{L79*/L79*}$* (right) retinas at e16. (B) Flat mount retinas at P0 show an ingrowth of the primary vascular plexus in controls (left top and bottom). In *ISPD$^{L79*/L79*}$* retinas (right top and bottom), the ingrowth of the primary plexus into the retina is delayed (arrow) and there is a persistence of hyaloid vasculature. Scale bar 50 μm A, 500 μm B top, 100 μm B bottom.

Supplemental Figure 3: Deletion of *dystroglycan* throughout the developing retina results in migration defects. (A) Recombination pattern of *Rosa26-lox-stop-lox-TdTomato; Ai9* reporter (green) by *Six3^{cre}* shows expression throughout the retina and in axons at e13. (B). Recombination pattern of *Rosa26-lox-stop-lox-TdTomato; Ai9* (green) by *Nestin^{cre}* shows expression in a sparse population of differentiated retinal neurons at e13. (C). Focal migration defects (arrowheads) in P7 *DG$^{F/-}$; Six3^{cre}* retinas are present across the entire span of the retina. Scale bar 100 μm A, B, left, 500 μm C, left, 50 μm A, B, C, right.

Supplemental Figure 4: Lamination of outer retina is normal in *dystroglycan* mutants. Photoreceptors (recoverin, green) have normal lamination in P14 *DG$^{F/-}$; Six3^{cre}* retinas (right). Scale bar 50 μm.

Supplemental Figure 5: Recombination pattern of *Isl1^{cre}* in the retina. Recombination pattern of *Rosa26-lox-stop-lox-TdTomato; Ai9* reporter (green) by *Isl1^{cre}* by shows expression in a large proportion of differentiated ganglion cells at e12.5 (left) and P0 (right). Dashed line indicates ILM. Asterisk notes a differentiated ganglion cell body that is still migrating toward the ILM. Scale bar 20 μm left panel, scale bar 50 μm right panel.